Age, geochemistry, and origin of the mid-Proterozoic Häme mafic dyke swarm, southern Finland

Luttinen, Arto

2022-06-10

Luttinen , A , Lehtonen , E , Bohm , K , Lindholm , T M , Söderlund , U & Salminen , J 2022 , ' Age, geochemistry, and origin of the mid-Proterozoic Häme mafic dyke swarm, southern Finland ' , Bulletin of the Geological Society of Finland , vol. 94 , no. 1 , pp. 75-101 . https://doi.org/10.17741/bgsf/94.

http://hdl.handle.net/10138/344801
https://doi.org/10.17741/bgsf/94.1.004

Bulletin of the Geological Society of Finland, Vol. 94, 2022, pp 75–102 https://doi.org/10.17741/bgsf/94.1.004

Age, geochemistry, and origin of the mid-Proterozoic Häme mafic dyke swarm, southern Finland

VERTAISARVIOITU
KOLLEGIALT GRANSKAD
PEER-REVIEWED
www.tsv.fi/tunnus

Arto Luttinen[1], Elina Lehtonen[2], Katja Bohm[2,3], Tanja Lindholm[2,4,5], Ulf Söderlund[6,7] and Johanna Salminen[2,8*]

[1]*Finnish Museum of Natural History, P.O. Box 44, FI-00014, University of Helsinki, Finland*

[2]*Department of Geosciences and Geography, P.O. Box 64, FI-00014 University of Helsinki, Finland.*

[3]*Department of Earth Sciences, Uppsala University, Villavägen 16, SE-752 36 Uppsala, Sweden*

[4]*Helsinki University Library, P.O. Box 53, FI-00014 University of Helsinki, Finland*

[5] *Research stations, P.O. Box 65, FI-00014 University of Helsinki, Finland*

[6]*Department of Geology, Lund University, Sölvegatan 12, SE-223 62 Lund, Sweden*

[7]*Department of Geosciences, Swedish Museum of Natural History, SE-10405 Stockholm, Sweden*

[8]*Geological Survey of Finland, P.O. Box 96, FI-02151 ESPOO*

Abstract

We have reappraised the age and composition of the mid-Proterozoic Häme dyke swarm in southern Finland. The dominant trend of the dykes of this swarm is NW to WNW. Petrographic observations and geochemical data indicate uniform, tholeiitic low-Mg parental magmas for all of the dykes. Nevertheless, the variability in incompatible trace element ratios, such as Zr/Y and La/Nb, provides evidence of changing mantle melting conditions and variable crustal contamination. Our ID-TIMS $^{207}Pb/^{206}Pb$ ages for four low-Zr/Y-type dykes indicate emplacement at 1639 ± 3 Ma, whereas the most reliable previously published ages suggest emplacement of the high-Zr/Y-type dykes at 1642 ± 2 Ma. We propose that the Häme dyke swarm, and possibly also the other mid-Proterozoic mafic dyke swarms in southern Finland, records a progressive decrease in Zr/Y values due to magma generation under developing areas of thinned lithosphere. We consider that the formation of mafic magmas was most probably associated with the upwelling of hot convective mantle in an extensional setting possibly related to the nearby Gothian orogeny. The generation of tholeiitic magmas below continental lithosphere was probably promoted by the elevated mantle temperature underneath the Nuna supercontinent. We speculate that the origin of most of the relatively small mid-Proterozoic mafic dyke swarms, anorthosites, rapakivi granites, and associated rocks found across Nuna was similarly triggered by extensional plate tectonics and the convection of anomalous hot upper mantle below the supercontinent.

Keywords: ID-TIMS, geochronology, rapakivi magmatism, mafic dyke, mid-Proterozoic, Fennoscandia

*Corresponding author (e-mail: johanna.salminen@gtk.fi)

Editorial handling: Jarmo Kohonen (e-mail: jarmo.kohonen@gtk.fi)

1. Introduction

Understanding of the globally widespread occurrences of ca. 1800–1000 Ma mafic and silicic intrusions, including massif-type anorthosite batholiths, is a well-known problem in geosciences (e.g. Hoffman 1989; Rämö & Haapala 1995; Vigneresse 2005; Ashwal & Bybee 2017; Klausen & Nilsson 2019). These mid-Proterozoic igneous rocks and provinces were formed across the Nuna (Columbia) supercontinent and they are frequently referred to as anorogenic suites, although their formation may be intimately linked to the lithospheric response to orogenic processes in nearby regions (e.g. Åhäll et al. 2000) or the collapse tectonics of an ancient orogen (Windley 1993). In this study, we collectively refer to these suites as within-plate magma systems, although they may also occur relatively close to active plate margins. Many of the within-plate magma systems are recognized as bimodal rapakivi granite associations exhibiting an age range of ~1700–1300 Ma (e.g. Emslie 1978; Windley 1993; Åhäll & Connelly 1998; Karlstrom et al. 2001). Episodic bimodal igneous activity resulted from the production of mantle-sourced magmas and subsequent melting of continental crust by the ascending mafic magmas (e.g. Rämö & Haapala 1995; Frost & Ronald Frost 1997; Heinonen et al. 2010a). The volcanic rocks of the mid-Proterozoic rapakivi-related igneous provinces are generally poorly preserved, and current views on the magma systems are mainly based on studies of plutons and dyke swarms (e.g. Rämö & Haapala 1995; Ashwal & Bybee 2017).

In the Fennoscandian Shield, the formation of the mafic and silicic rocks of the rapakivi association commenced ca. 100 Myr after the termination of the Svecofennian orogenic activity (e.g. Heinonen et al. 2010a). The mid-Proterozoic rapakivi-related igneous province of southern Finland is formed of several rapakivi granite plutons, a few mafic plutons, and several silicic and mafic dyke swarms (Fig. 1). Rare exposures of coeval volcanic rocks are found in the northeastern Lake Ladoga area, on the island of Suursaari, and in megaxenoliths within the Wiborg batholith (Rämö & Haapala 2005). The mafic Häme dyke swarm has been regarded to represent the onset of rapakivi-related mid-Proterozoic magmatism in Fennoscandia (e.g. Rämö & Haapala 2005). Accordingly, the emplacement history and geochemical composition of the Häme dyke swarm provide critical evidence for the mantle sources (e.g. plume vs. non-plume), magma transport mechanisms, and tectonic events involved in rapakivi-related magmatism.

Based on studies by Laitakari (1987) and Vaasjoki & Sakko (1989), the Häme dyke swarm is interpreted to constitute distinctive sets of dykes differing in strike, age, and composition (see also Laitakari 1969). It was suggested that the dykes trending ca. 90–105°E are older (ca. 1.67 Ga) than those trending ca. 120–135°E (ca. 1.65 Ga). We refer to these sets, respectively, as the WNW-trending and NW-trending sets. Dykes of the WNW-trending set are more olivine rich (Laitakari 1987; Laitakari & Leino 1989) and have lower differentiation indices than the NW-trending set (Laitakari 1969). Furthermore, the WNW-trending set has been described as lacking plagioclase phenocrysts and megacrysts that occur abundantly in the NW-trending set. Overall, the scenario of two chronologically and compositionally distinctive sets of mafic dykes is a key component of the current genetic model for the bimodal rapakivi association of the Fennoscandian Shield (Rämö & Haapala 2005).

A careful review of the available data reveals ambiguities in this conventional scenario, however. First, field evidence of the relative ages, e.g. cross-cutting relationships, of the two dyke sets has not been recorded (Laitakari 1987). Second, the U–Pb age data from the 1980s and 1990s are compromised by the predominance of discordant results, heterogeneous zircon and baddeleyite populations, and insufficient documentation. Third, in the absence of comprehensive age data, the chronological interpretation has largely been influenced by the assumption that the olivine-rich dykes are more primitive, and thus likely to be older than the olivine-poorer and plagioclase phenocryst-

bearing dykes (e.g. Laitakari 1987). Examination of the compositional data for the Häme dyke swarm reveals that the purported compositional dichotomy between the two sets is founded on only a few geochemical analyses and biased sampling of only a small number of large dykes. Furthermore, the abundance of olivine probably relates to in situ differentiation and is unrelated to parental magma compositions and relative ages.

In this work, we reappraise the age and composition of the Häme dyke swarm. We provide new U–Pb isotope dilution thermal ionization mass spectrometry (ID-TIMS) ages for four mafic dykes and report major and trace element data for 66 dykes across the swarm. We use our results to test the conventional division of the dykes of the Häme swarm into two groups. We also use data on the Suomenniemi, Sipoo, Kopparnäs, Åland, and Satakunta dyke swarms (Rämö 1991; Luttinen & Kosunen 2006; Bohm 2018) and associated rapakivi granites (e.g. Rämö 1991; Laitakari et al. 1996; Kosunen 1999; Rämö & Haapala 2005) to discuss the chronology and origin of rapakivi-related magmatism in southern Finland. Finally, we briefly evaluate the geodynamic environment of rapakivi-related mafic magmatism in Fennoscandia and possible implications for mid-Proterozoic within-plate mafic magmatism worldwide.

2. Geological background

The Häme dyke swarm is situated WNW of the Wiborg rapakivi batholith and occupies an area of 20 x 170 km. The dykes cross-cut the Svecofennian supracrustal and intrusive rocks in southern Finland (Fig. 1). The multiphased Svecofennian orogenic evolution started at ca. 1920 Ma (Lahtinen et al. 2005) and ended at ca. 1800–1750 Ma with the collapse of the orogen (e.g. Lahtinen et al. 2005; Nikkilä et al. 2016). The period of gravitational collapse was associated with the rapid uplift of the metamorphic crust (e.g. Korsman et al. 1999) and widespread emplacement of bimodal shoshonite-granite intrusions, probably due to delamination of the continental lithospheric mantle (e.g. Väisänen et al. 2000). The intrusion of the Häme dyke swarm occurred more than 120 Myr after the main phase of the Svecofennian igneous activity. The scattered occurrences of ultramature quartz arenitic sandstones and conglomerates that were deposited over the Svecofennian basement and are also found as xenoliths in the Häme dykes, indicate fully cratonized conditions prior to the onset of the mid-Proterozoic bimodal magmatism (e.g. Pokki et al. 2013). After the collapse of the Svecofennian orogen, the next major tectono-magmatic evolutionary stage was the emplacement of the rapakivi granites and related mafic and silicic rocks (Rämö & Haapala 2005). The rapakivi granites were intruded during two main phases at ca. 1650–1620 Ma in southeastern Finland (e.g. Vaasjoki 1977; Laitala 1984; Törnroos 1984; Vaasjoki et al. 1989; Heinonen et al. 2010a; Rämö & Mänttäri 2015; Heinonen et al. 2016; Heinonen et al. 2017) and at ca. 1590–1535 Ma in southwestern Finland and in the Lake Ladoga area, Russian Karelia (e.g. Vaasjoki 1977; Idman 1989; Suominen 1991; Lindberg & Bergman 1993; Lehtonen et al. 2003).

The rapakivi batholiths of southern Finland are associated with both mafic and silicic dykes (e.g. Rämö 1991; Laitakari et al. 1996; Kosunen 1999; Rämö & Haapala 2005). The older group of rapakivi batholiths (Wiborg, Suomenniemi, Ahvenisto, Onas, Bodom, and Obbnäs) is associated with the Häme and Suomenniemi swarms and the much smaller Kopparnäs and Sipoo swarms, whereas the younger rapakivi batholiths in southwestern Finland (Vehmaa, Laitila, Eurajoki, and Åland) are spatially associated with the Åland–Åboland and Satakunta swarms (Fig. 1). In the Satakunta swarm, a subgroup of NW- to WNW-trending dykes has been tentatively correlated with the Häme swarm on the basis of paleomagnetic results (Salminen et al. 2014; Salminen et al. 2017). In general, the lack of cross-cutting mafic dykes in the silicic plutons and the cross-cutting rapakivi granite in the 1643 ± 5 Ma (Siivola 1987) Lovasjärvi gabbroic intrusion suggest that the emplacement of mafic magmas commenced before the formation of

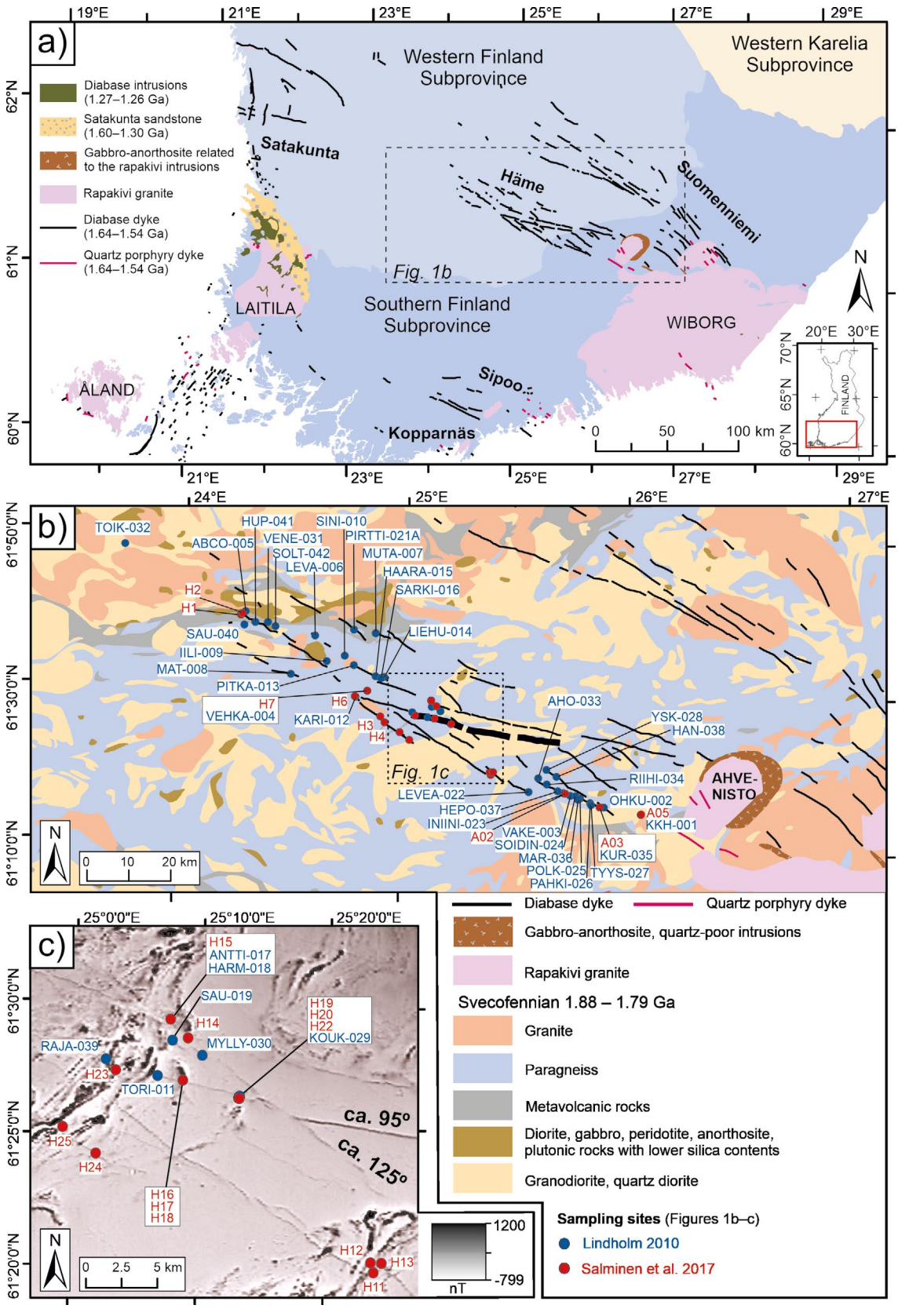
a)
Diabase intrusions (1.27–1.26 Ga)
Satakunta sandstone (1.60–1.30 Ga)
Gabbro-anorthosite related to the rapakivi intrusions
Rapakivi granite
Diabase dyke (1.64–1.54 Ga)
Quartz porphyry dyke (1.64–1.54 Ga)
Western Finland Subprovince
Western Karelia Subprovince
Satakunta
Häme
Suomenniemi
Fig. 1b
LAITILA
Southern Finland Subprovince
WIBORG
ÅLAND
Sipoo
Kopparnäs
0 50 100 km
FINLAND
b)
TOIK-032
HUP-041
SINI-010
ABCO-005
VENE-031
PIRTTI-021A
SOLT-042
MUTA-007
LEVA-006
HAARA-015
SARKI-016
H2
H1
SAU-040
LIEHU-014
IILI-009
MAT-008
PITKA-013
H7
VEHKA-004
H6
KARI-012
H3
H4
AHO-033
YSK-028
HAN-038
Fig. 1c
RIIHI-034
AHVE-NISTO
LEVEA-022
OHKU-002
A05
HEPO-037
KKH-001
ININI-023
A02
VAKE-003
SOIDIN-024
A03
KUR-035
MAR-038
POLK-025
TYYS-027
PAHKI-026
0 10 20 km
c)
H15
ANTTI-017
HARM-018
SAU-019
H19
H20
H22
KOUK-029
H14
RAJA-039
MYLLY-030
H23
TORI-011
ca. 95°
ca. 125°
H25
H24
H16
H17
H18
H12
H13
H11
0 2.5 5 km
1200
-799
nT
Diabase dyke
Quartz porphyry dyke
Gabbro-anorthosite, quartz-poor intrusions
Rapakivi granite
Svecofennian 1.88 – 1.79 Ga
Granite
Paragneiss
Metavolcanic rocks
Diorite, gabbro, peridotite, anorthosite, plutonic rocks with lower silica contents
Granodiorite, quartz diorite
Sampling sites (Figures 1b–c)
Lindholm 2010
Salminen et al. 2017

silicic plutons (Laitakari 1969; Eklund et al. 1994). Nevertheless, abundant field evidence of mingling and mixing indicates bimodal magmatism and an intimate genetic relationship between silicic and mafic magmas (e.g. Eklund et al. 1994; Rämö & Haapala 1995; Fred et al. 2019).

The Wiborg rapakivi batholith has U–Pb ages ranging from 1646 ± 4 Ma (Rämö et al. 2014) to 1627 ± 3 Ma (e.g. Rämö et al. 2014; Heinonen et al. 2016; Heinonen et al. 2017). Based on U–Pb ages on zircons in the matrix and potassium feldspar megacrysts in the main granite types, Heinonen et al. (2017) suggested that the Wiborg rapakivi batholith crystallized during at least two stages at ca. 1636–1628 Ma and at ca. 1628 Ma. Three intrusions of the Häme dyke swarm have previously been dated using the U–Pb method on zirconium minerals: (1) The WNW (95°E)-trending Virmaila dyke has yielded ID-TIMS multigrain baddeleyite ages of 1667 ± 9 Ma (concordia age, Vaasjoki et al. 1991) and 1642 ± 2 Ma ($^{207}Pb/^{206}Pb$ age; Salminen et al. 2017). (2) The NW (120–135°E)-trending Ansio and Heinola dykes yielded a combined ID-TIMS multigrain zircon age of 1646 ± 6 Ma (intercept age; Laitakari 1987). (3) The WNW (90°E)-trending Torittu dyke has yielded a laser-ablation multicollector inductively coupled mass spectrometry (LA-MC-ICPMS) baddeleyite age of 1647 ± 14 Ma ($^{207}Pb/^{206}Pb$ age; Salminen et al. 2017).

Figure 1. a) A geological overview of southern Finland. The subprovinces are after Nironen (2017). Major rapakivi batholiths and dyke swarms are indicated. b) Geological map of the Häme dyke swarm region. The simplified lithology is drawn after Bedrock of Finland 1:1 000 000, Geological Survey of Finland (CC BY 4.0). The widths of the dykes are exaggerated. The dyke with a "spotted" texture is indicated with a thick black line (see section 5.2.). c) Aeromagnetic anomaly map showing the two predominant WNW (ca. 95°) and NW (ca. 125°) trends of the dykes. Map layer: Aeromagnetic anomaly map of Finland, Geological Survey of Finland (Open license). Sampling sites in b) and c) after Lindholm (2010) and Salminen et al. (2017). The sampling codes are listed in Electronic Appendix A.

3. Sampling and methods

3.1. Sampling

The widths of the vertical to subvertical dykes of the Häme swarm vary across the dyke swarm from a few centimeters up to 250 m, and the dykes are widest near the Wiborg batholith (e.g. Laitakari 1969, 1987). Crystallization of zircon and baddeleyite in mafic magmas occurs close to solidus temperatures, and the largest grains are likely to be found within granophyric patches of slowly cooled intrusions. We sampled four wide dykes for U–Pb geochronology: one 12-meter-wide dyke trending WNW (95°E) in Hirtniemi (H12) and three >40-meter-wide dykes trending NW (130–135°) in Hirtniemi (H13), Myllylahti (H14), and Muorinkallio (H25) (Fig. 1). Block samples were taken from the coarse-grained central part of the dyke using a rock hammer.

The geochemical compositions of parental magmas are best preserved in rapidly cooled dykes. Accordingly, our geochemical samples of 66 dykes of the Häme dyke swarm were mainly collected from the margins of the dykes. These geochemical studies were carried out in conjunction with two MSc projects (Fig. 1). Block samples of 44 dykes were taken in 2008 (Lindholm 2010) and 22 dykes were sampled with a portable drill during paleomagnetic field campaigns in 2009, 2014, and 2016 (Salminen et al. 2017; Bohm 2018).

3.2. Geochronological method

We separated baddeleyite from crushed rock using the water-based separation technique at the Department of Geology, Lund University, Sweden, following the procedure described in detail by Söderlund & Johansson (2002). The best grains of baddeleyite (i.e. transparent grains with no visible inclusions or zircon overgrowths) were hand-picked under an optical microscope. Baddeleyite grains from all samples share similar features of dark brown, rod-shaped crystals with no signs of secondary overprint, such as frosty zircon rims. A single grain from dykes H12 and H13, and three

grains from dykes H14 and H25 were selected for geochronology and were transferred to Teflon capsules in ethanol. The grains were washed repeatedly in ultrapure 7 M HNO_3 and H_2O to minimize the Pb blank. For dissolution, an ultrapure HF:HNO_3 (10:1) solution was added to the individual Teflon capsules together with 1 drop of ^{205}Pb–$^{233\text{-}236}U$ tracer solution. The capsules were mounted in steel jackets before being placed in an oven for 72 hours at 190 °C. The capsules with dissolved grains were then put on a hot plate for evaporation. After evaporation, 10 drops of ultrapure 6 M HCl together with 1 drop of 0.25 M H_3PO_4 were added to each capsule to redissolve and then left to evaporate on a hot plate. Silica gel was added to each of the fractions before loading on outgassed Re filaments.

The U and Pb isotopic compositions were measured on a Thermo Scientific - Finnigan TRITON mass spectrometer at the Department of Geosciences in the Swedish Museum of Natural History. Peak intensities were measured using a secondary electron multiplier in dynamic (peak jumping) mode. Pb and U isotopic data were collected in the temperature range of 1210–1240 °C and 1310–1360 °C, respectively. Uranium decay constants are from (Jaffey et al. 1971; Steiger & Jäger 1977). Isotopic ratios were corrected for a total procedural blank of 0.04 pg for U and 0.4 pg for Pb. Mass fractionation for Pb was determined by replicate analyses of the common and radiogenic NIST standard reference materials SRM 981 and SRM 983. The determination of U fractionation was directly obtained from the measured $^{233}U/^{236}U$ isotopic ratio.

The U–Pb concordia plots were prepared and ages calculated using Isoplot version 3.7 (Ludwig 2003). The Stacey & Kramers (1975) common Pb evolution model was used to estimate the initial Pb compositions. The uncertainty in age includes ±0.04 in Pb fractionation and ±50 % in the Pb and U blank concentration. Uncertainties in the Pb blank composition are 2.0 % for $^{206}Pb/^{204}Pb$ and 0.2 % for $^{207}Pb/^{204}Pb$.

3.3. Geochemical analyses

The samples were prepared for geochemical analyses at the Helsinki geophysical, environmental and mineralogical laboratories (HelLabs) of the Department of Geosciences and Geography, University of Helsinki. The samples were broken inside tough plastic material with a hydraulic press and a hammer. The large block samples were further disintegrated using a jaw crusher. Approximately 30 g of representative fragments were carefully hand-picked to avoid contamination from the processing tools. The selected chips were pulverized using a tungsten carbide ball mill at 350 rpm for 10+5 min. Glass beads for the X-ray fluorescence (XRF) analyses were prepared from a 1:10 mixture of sample and flux (equal amounts of lithium tetraborate and lithium metaborate and 0.5 % lithium bromide). The glass beads were produced by fusing the powder mixture in a 1000 °C gas flame with a Claisse M4 fluxer using Pt–Au crucibles and molds (95 % Pt, 5 % Au). The subset of 22 drill-core samples (codes start with JS or H) was analyzed with a PANalytical Axios mAX WD-XRF spectrometer equipped with a Rh-anode X-ray tube at the 4 kW power setting. The 44 block samples were analyzed for major and trace elements using a Philips PW1480 X-ray spectrometer. The analytical procedure was similar to that described above with the exception of a slightly different flux (1.0 % instead of 0.5 % lithium bromide). The XRF analyses of the major element oxides and trace elements (Ba, Ce, Cu, Cr, La, Nb, Ni, Sr, Rb, U, V, Zn, Zr, Y) were calibrated using Certified Reference Material rock powders that were fused into beads. The precision for major element oxides was estimated to be better than 0.1 wt % and for trace elements better than 10 ppm, whereas the accuracy was in the order of <5 % for major elements and <20 % for trace elements (Rämö et al. 2016). The quantitative results were calculated with SuperQ 5.3 using fixed alpha theoretical matrix correction factors and selected line-overlap corrections.

All of the block samples were analyzed for trace elements (REE, Ba, Th, Nb, Y, Hf, Ta, U, Pb, Rb, Cs, Sr, Sc, Zr) using an inductively-coupled plasma source mass spectrometer (ICP-MS) at the Peter Hooper GeoAnalytical Laboratory, University of Washington, using a protocol described in Knaack et al. (1994). References for the analytical methods at the GeoAnalytical Laboratory are given in https://environment.wsu.edu/facilities/geoanalytical-lab/technical-notes/icp-ms-method/. Repeated measurements of an incompatible element-poor standard suggested precision of ≤2 % for most elements, ≤5 % for Nb and La, and ≤10 % for Ta, Rb, Cs, Th, U, and Pb. Results obtained using ICP-MS were favored over XRF data in the case of the block samples.

Comparison between the two subsets of data does not indicate systematic bias (Electronic Appendix B). The use of a steel jaw crusher and tungsten carbide mill may have caused minor contamination with Fe, Co, and Ta. We used GCDkit 6.0 (Janoušek et al. 2006) to plot the whole-rock geochemical data on diagrams and to calculate the CIPW normative compositions.

4. Results

4.1. Petrography

Based on field observations and thin section analyses, the majority of the studied dykes are plagioclase porphyritic and the rest are aphyric (Fig. S1 in Electronic Appendix C). In some samples, abundant plagioclase phenocrysts form glomerocrysts. The groundmass typically shows ophitic, sub-ophitic, or nesophitic textures, depending on the relative size of euhedral plagioclase laths and clinopyroxene. Some samples from the dyke margins have a hyalophitic texture with the microcrystalline, feldspathic mesostasis representing devitrified glass. Nearly half of the dykes contain olivine in the groundmass. The Fe–Ti groundmass oxides are frequently acicular or skeletal and rarely equant. In the coarse-grained samples, groundmass oxides are typically partially rimmed by biotite, and apatite and zircons can be recognized in a few of them. One of the >40-m-wide dykes (JS14-H14) contains orthopyroxene, which is partially mantled by clinopyroxene, but clinopyroxene also occurs within poikilitic groundmass plagioclase. A MgO-rich sample, AO5-B, contains abundant small olivine grains in poikilitic clinopyroxene. Groundmass clinopyroxene shows brown pleochroism typical of Ti-rich rocks and olivine has yellowish-greenish-reddish pleochroism. Most of the samples are relatively unaltered, so that the plagioclase phenocrysts contain small amounts of sericite, olivine is partially altered to iddingstite/bowlingite (?), and biotite is partially altered to chlorite. A few samples contain small amygdules variably comprised of carbonate, quartz, and chlorite. Notably, samples representing the two main strike directions show similar textures and modal compositions.

4.2. Dyke trends

The strike trends of the studied dykes (47 measurements; Electronic Appendix A and Fig. S2 in Electronic Appendix C) display an overall bimodal distribution with maxima corresponding to 110–115° and 140–145°. Several dykes have nearly perpendicular strike directions relative to the two dominant groups. In the following, we have divided the dykes into a NW-trending group (strikes 120–140°; includes most of the dykes) and a WNW-trending group (strikes 90–110°). We correlate the 120–140° trending dykes and the 90–110° trending dykes with the NW and WNW sets of dykes identified by Laitakari (1969, 1987).

4.3. U–Pb geochronology

Our new U–Pb baddeleyite age data for the Häme swarm are listed in Table 1. A concordia diagram with 2σ error ellipses is presented in Figure 2. All data plot concordantly to near-concordantly.

Table 1. U–Pb baddeleyite geochronology data for the mafic dykes of the Häme dyke swarm

Sample (number of grains)	U/Th	Pbc/ Pbtot[1)]	$^{206}Pb/^{204}Pb$ raw[2)]	$^{207}Pb/^{235}U$ [corr][3)]	± 2σ % err	$^{206}Pb/^{238}U$ [corr][3)]	± 2σ % err	$^{207}Pb/^{235}U$ [age, Ma]	$^{206}Pb/^{238}U$ [age, Ma]	$^{207}Pb/^{206}Pb$ [age, Ma]	± 2σ % [%]	Concordance [%]
H12 (1 grain)	18,3	0,299	165,5	4,0285	0,56	0,28963	0,47	1640,0	1639,7	1640,4	5,8	100,0
H13 (1 grain)	32,5	0,018	3548,7	3,9912	0,29	0,28727	0,27	1632,4	1627,9	1638,3	2,1	99,4
H14 (3 grains)	19,2	0,036	1723,4	3,8945	0,28	0,28066	0,25	1612,5	1594,7	1635,9	2,5	97,5
H25 (3 grains)	29,5	0,087	743,2	4,0132	0,95	0,28931	0,92	1636,9	1638,1	1635,3	6,2	100,2

1) Pbc = common Pb; Pbtot = total Pb (radiogenic + blank + initial).

2) Measured ratio, corrected for fractionation and spike.

3) Isotopic ratios corrected for fractionation (0.1 % per amu for Pb), spike contribution, blank (0.4 pg Pb and 0.04 pg U), and initial common Pb. Initial common Pb corrected with isotopic compositions from the model of Stacey and Kramers (1975) at the age of the sample.

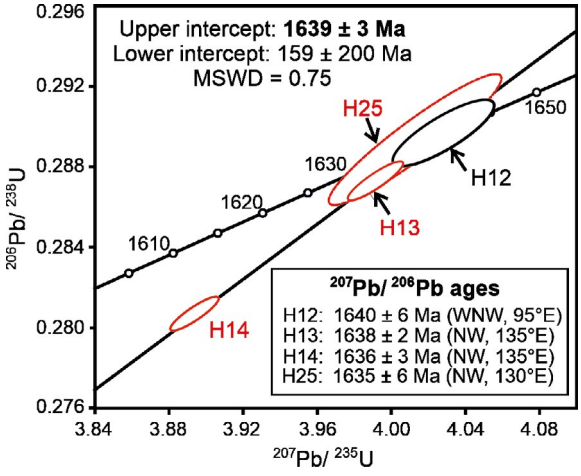

Figure 2. U–Pb concordia diagram of age-determined samples from the Häme dyke swarm. Error ellipses and age uncertainties are given at 2σ. The interpreted emplacement ages are presented in the inserted box.

In the case of the WNW-trending dyke H12 (strike 95°E), a single concordant baddeleyite grain from Hirtniemi yielded a $^{207}Pb/^{206}Pb$ age of 1640 ± 6 Ma. A concordant baddeleyite fraction (3 grains) from the NW-trending dyke H25 (strike 130°E) in Muorinkallio indicates a marginally younger $^{207}Pb/^{206}Pb$ age of 1635 ± 6 Ma. The nearly concordant baddeleyite fraction (1 grain) from the NW-trending dyke H13 (strike 135°) in Hirtniemi yielded a $^{207}Pb/^{206}Pb$ age of 1638 ± 2 Ma, whereas the discordant baddeleyite fraction (3 grains) from the NW-trending dyke H14 (strike 135°) in Myllylahti yielded a $^{207}Pb/^{206}Pb$ age of 1635 ± 3 Ma. A linear regression through these four baddeleyite fractions yielded an upper intercept age of 1639 ± 3 Ma and an imprecise lower intercept age of 159 ± 200 Ma (MSWD = 0.75) (Fig. 2).

4.4. Geochemistry

Geochemical data were obtained for 69 samples representing 66 dykes. The geochemical compositions of our samples are illustrated in Figures 3–4 and the dataset is listed in Electronic Appendix B. In the total alkali vs. silica diagram, the Häme dykes define a tight cluster along the alkaline–subalkaline boundary, with most of the samples plotting within the field of basalt, and a few samples can be classified as picrobasalt, trachybasalt, basaltic trachyandesite, and basaltic andesite (Fig. S3 in Electronic Appendix C). The CIPW norm indicates olivine (n = 43) and quartz tholeiitic (n = 26) compositions (Electronic Appendix B). The dykes have relatively high TiO_2 contents (mainly 2–4 wt%) and can be characterized as high-Ti tholeiites typical of many continental flood basalt suites (e.g. Cox et al. 1967; Bellieni et al. 1984; Pik et al. 1998).

The studied dykes exhibit wide ranges for MgO (ca. 3–16 wt.%) and the Mg number (31–62; molar 100*Mg/[Mg+Fe^{2+}]), where Fe^{2+}=0.9*total Fe), but most of the samples have a low MgO content and Mg number. The concentrations of SiO_2, TiO_2, K_2O, and P_2O_5 show negative correlations with the Mg number, whereas those of Al_2O_3 and CaO correlate positively with low Mg numbers (<40) and record scattered, but generally decreasing values when Mg numbers are relatively high (Fig. 3). The concentrations of FeOtot, Na_2O, and MnO do not correlate with the Mg number. The trace element contents show notable variability. Most of the mantle-incompatible elements (e.g. Ba, Rb, Zr, Nb, La, Ce, Y) correlate negatively with the Mg number,

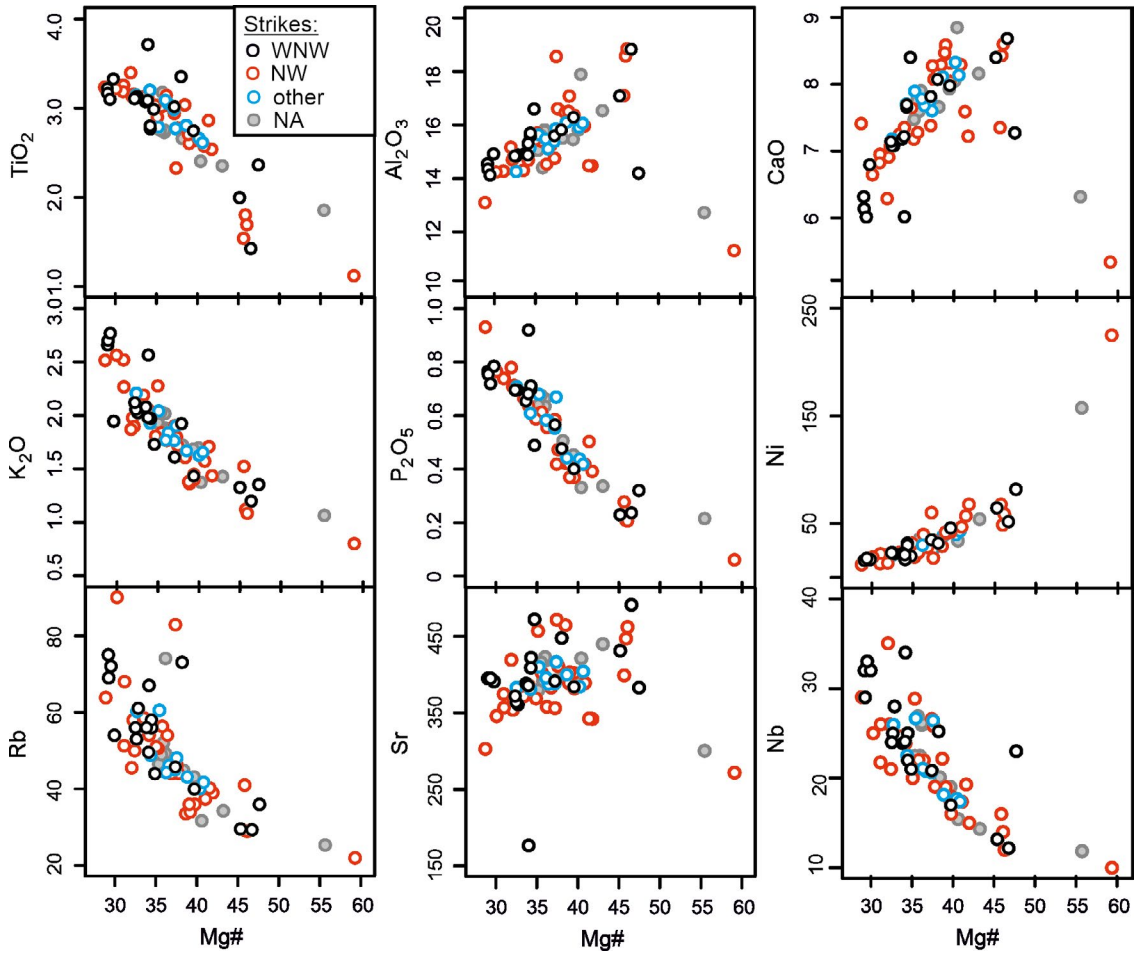

Figure 3. Variations in the major element oxide (wt.%) and trace element (ppm) contents vs. the Mg number (Mg#). Dyke strikes: WNW: 90–110 °E; NW: 120–140 °E; Other: other strike directions; NA: strike not available.

whereas mantle-compatible Ni and Cr correlate positively with the Mg number, although the latter shows a large scatter at high Mg numbers (Fig. 3). The chalcophile Cu and Zn and plagioclase-compatible Sr show considerable scatter, but Zn correlates negatively with the Mg number and the variation in Sr resembles that of Al_2O_3 (Fig. 3).

The analysis of rare earth elements (REE) for 41 representative samples indicated uniformity (Fig. 4a). The samples are enriched in light REE, with chondrite-normalized $(La/Sm)_N$ varying from 2.1 to 3.2, and depleted in heavy REE, with $(Sm/Lu)_N$ varying from 2.4 to 3.9. Most of the samples display a minor negative Eu anomaly and Eu/Eu* ($Eu/Eu^* = Eu_N/\sqrt{[(Sm_N)\cdot(Gd_N)]}$) varies from 0.76 to 1.10. The primitive mantle-normalized incompatible element patterns display a general enrichment from Lu towards Cs, but several elements record negative (Sr, Ti) or positive (Cs, Pb) anomalies and the mantle-normalized contents of Th, U, and Nb are lower than those of light REE (Fig. 4b). As in many continental flood basalt suites, the ratios of incompatible elements in the Häme dykes show similarities with upper continental crust (e.g. La/Nb 1.5–2.4, Th/Nb 0.12–0.22, Ce/Pb 0.08–0.1).

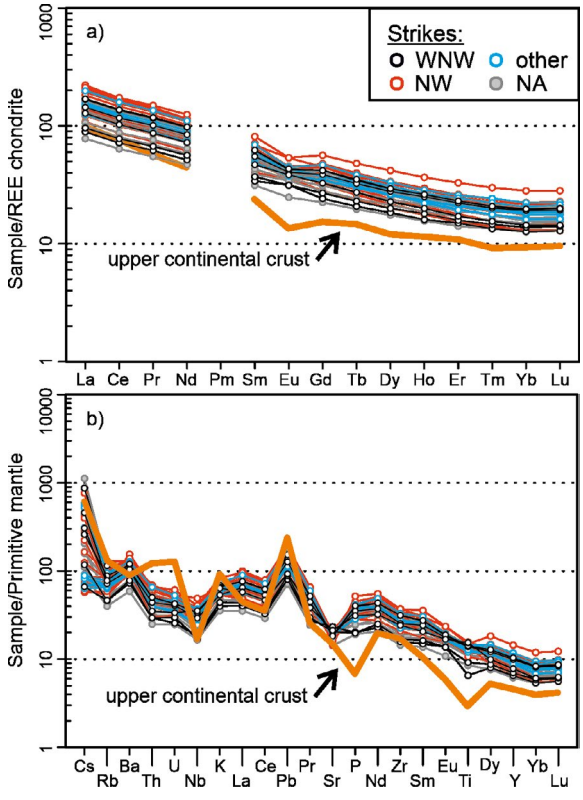

Figure 4. Incompatible element compositions in a) a chondrite-normalized REE diagram (normalized after Boynton 1984) and b) a primitive mantle-normalized diagram (normalized after Sun & McDonough 1989). The average composition of the upper continental crust (Rudnick & Gao 2003) is presented for comparison. Dyke strikes: WNW = 90–110 °E; NW = 120–140 °E; Other: other strike directions; NA: strike not available.

5. Discussion

We start our discussion by addressing the causes of compositional variability in the Häme dyke swarm and use geochemical data from this study and Rämö (1991) to constrain the mantle source characteristics of the mafic magmas. Thereafter, we critically evaluate the purported compositional difference between the predominant NW and WNW sets of dykes and summarize the available age constraints on the Häme dykes and other mafic and silicic rock types that are temporally and spatially associated with the Wiborg rapakivi batholith. Finally, we use available geochemical and chronological data to present a new scheme for the origin of the rapakivi-related dyke swarms in southern Finland and briefly discuss the possible roles of lithospheric processes and large-scale mantle convection in the generation of mid-Proterozoic within-plate mafic magmatism worldwide.

5.1. Magmatic differentiation and mantle source

Our samples exhibit notably uniform basaltic compositions, and the variable major and trace element contents can be readily ascribed to fractional crystallization of olivine and plagioclase in the magma transport system (Figs. 3–4). For example, the decrease in Al_2O_3 and CaO with decreasing MgO can be attributed to the combined fractionation of olivine and plagioclase from parental magmas that had MgO contents of ca. 5 wt.% and Al_2O_3 contents of ca. 16 wt. %, whereas the decrease in Al_2O_3 when MgO increases from 5 to 16 wt.% is compatible with olivine fractionation (Fig. 5). However, the presence of abundant iron-rich olivine (Fo_{52}; Laitakari 1969) in the MgO-rich Partakorpi dyke (8–11 wt.%; this study and Petri Peltonen, personal communication) and the positive correlation between FeO_{tot} and MgO strongly suggest that the olivine- and MgO-rich samples record the accumulation of relatively iron-rich olivine in evolved magmas rather than fractional crystallization of magnesium-rich olivine from primitive magmas (Fig. 5a). We have illustrated the geochemical result of olivine accumulation by calculating the composition of olivine that would be in Mg–Fe equilibrium with a typical low-MgO Häme dyke sample (Fo_{68} when the basaltic melt has MgO = 4.8 wt.%) and by adding this olivine to the average dyke composition. The model provides a good fit to the data. In the same manner, the samples that are poor in FeO_{tot} and high in Al_2O_3 can be explained by the accumulation of plagioclase and olivine–plagioclase phenocryst assemblages in the dykes (Fig. 5). The variable trace element contents can be also ascribed to fractional crystallization and accumulation of

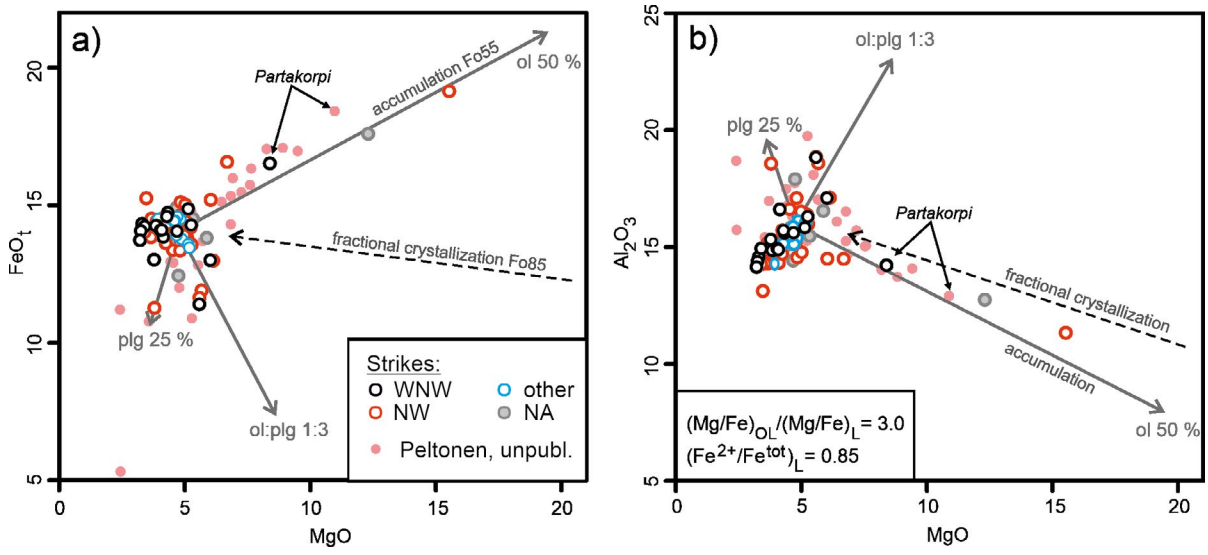

Figure 5. Variations in a) FeO_t and b) Al_2O_3 vs. MgO in the samples from the Häme dyke swarm. The accumulation trends for olivine (ol 50 %), plagioclase (plg 25 %), and olivine and plagioclase (ol:plg 1:3) are indicated as arrows. Dyke strikes: WNW = 90–110 °E; NW = 120–140 °E; Other: other strike directions; NA: strike not available. Samples from the Partakorpi dyke are indicated. Additional data for Häme dykes are from Petri Peltonen (personal communication).

the gabbroic olivine-pyroxene-plagioclase mineral assemblage (i.e. enrichment of most trace elements and variability in the Ni, Cr, and Sr contents). Overall, we regard that fractional crystallization and the accumulation of phenocrysts from geochemically uniform low-Mg basaltic parental magmas were mainly responsible for the variable major and trace element contents in the Häme dykes.

Our data and unpublished reference data (Petri Peltonen, personal communication) indicate that olivine accumulation only took place within the widest dykes (ca. >30 m; Laitakari 1969). It is interesting to note that olivine is found in the studied dykes in the groundmass only, and in many cases it is poikilitically enclosed within large clinopyroxene crystals (Fig. S1 in Electronic Appendix C). These observations suggest that olivine crystallized during or just prior to the emplacement of the parental magmas and that the Fe-rich crystals were only able to settle and accumulate within the magma column inside the widest dykes. The relatively Fe-rich compositions of the Häme dykes indicate that the melts had a high density, which explains the flotation and accumulation of plagioclase phenocrysts and macrocrysts in many of the dykes (e.g. Laitakari 1969).

A detailed analysis of the ratios of elements that are incompatible in the main minerals olivine, plagioclase, and clinopyroxene reveals variability that cannot be explained by crystal-melt differentiation alone. For example, the Häme dykes exhibit wide ranges of Zr/Y, Nb/Y, and La/Nb (Fig. 6). Highly variable Nb/Y and Zr/Y are generally compatible with the expected result of variable degrees of melting in the mantle source of these rocks, because Y is notably more compatible in garnet than Nb and Zr. However, partial melting of a homogeneous mantle source cannot explain variable ratios of similarly incompatible La and Nb (Fig. 6b). Given that the La/Nb values almost invariably exceed the range typical of oceanic high-Ti rocks (<1; Willbold & Stracke 2006), we consider that most of the sampled dykes include a high-La/Nb component derived from either continental crust or lithospheric mantle.

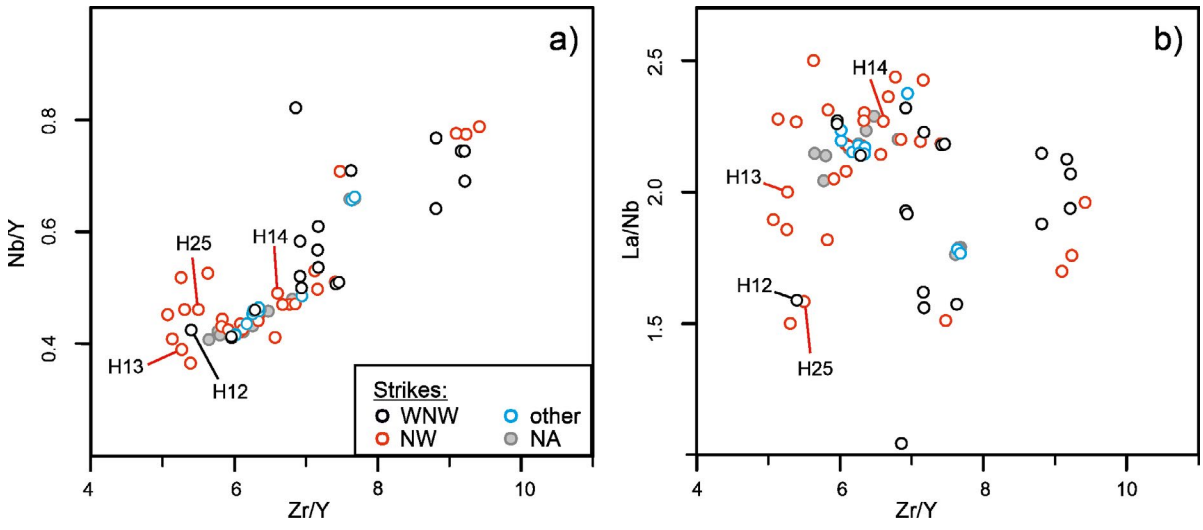

Figure 6. Variation in a) Nb/Y and b) La/Nb vs. Zr/Y in the samples of the Häme dyke swarm. The compositions of the dated dykes are indicated (H12, H13, H14, and H25). Dyke strikes: WNW = 90–110 °E; NW = 120–140°E; Other: other strike directions; NA: strike not available.

In the 1980s and 1990s, continental flood basalts that show geochemical affinities to continental crust were mainly ascribed to melting of metasomatically enriched lithospheric mantle (e.g. Hawkesworth et al. 1984; Rämö 1991), but recently developed thermodynamically constrained models suggest that mafic magmas are very likely to be geochemically overprinted by the assimilation of wall rocks (e.g. Heinonen et al. 2019). Moreover, the generation of large quantities of relatively dry tholeiitic magmas from either fertilized (wet) or depleted (dry) continental lithospheric mantle seems thermodynamically improbable (e.g. Arndt et al. 1993). Presently, lithospheric mantle is considered by many researchers to contribute to the origin of flood basalts as a highly incompatible element-enriched contaminant of magmas formed in the convective mantle (e.g. Ellam et al. 1992; Gibson et al. 1995; Riley et al. 2005; Luttinen et al. 2015). We consider that, in the case of the Häme dyke swarm, the marked similarity between the incompatible element patterns of the low-MgO dykes and upper continental crust (Fig. 4b) at least partly stems from the assimilation of crustal wall rocks. Consequently, the samples with the lowest Th/Nb and La/Nb values are likely to represent the least crustally contaminated magmas; these samples have high Nb, Ti, and Zr relative to Y and Yb, and they show affinities to typical OIB (e.g. Pearce 2008; Hollocher et al. 2012). Specifically, the primitive mantle-normalized incompatible element patterns of the least-contaminated Häme dykes with high Ba/La (mainly 14–18) and La/Nb (mainly 1.5–1.8) values and low values of Ce/Pb (<13) are quite similar to those of OIB associated with the so-called enriched mantle 1 (EM1) reservoir (e.g. Tristan da Cunha hotspot; Fig. S4 in Electronic Appendix C). While the exact identity of the mantle source of the Häme dykes is beyond the scope of this study, sparse isotopic data reported by Rämö (1991) for the Häme swarm (initial ε_{Nd} +0.6 to –0.2) and the Suomenniemi swarm (initial ε_{Nd} +1.6 to –1.2), and by Heinonen et al. (2010b) for olivine-bearing gabbroic rocks of the nearby Ahvenisto complex (initial ε_{Nd} +0.4 to +0.2, $^{87}Sr/^{86}Sr$ 0.7034 to 0.7035), lend support to the derivation of the parental magmas of these closely-spaced mafic intrusive suites from an EM1-type source (e.g. Tristan da Cunha modern values of ε_{Nd} ca. –4 to +4 and $^{87}Sr/^{86}Sr$ 0.7035 to 0.7055; Hoernle et al. 2015).

5.2. Compositional variability and different dyke strikes

In the previous literature, the Häme swarm has been regarded to be composed of two distinctive subsets that differ from each other in terms of age, strike, mineral mode, texture, and chemical composition. Specifically, the presumably older WNW-trending dykes have been described as compositionally relatively primitive olivine tholeiites that typically contain abundant olivine, but no plagioclase phenocrysts or large plagioclase fragments (Laitakari 1987; Laitakari & Leino 1989). The presumably younger NW-trending dykes have been described as compositionally relatively evolved dykes that are characterized by phenocrysts, megacrysts (up to <20 cm), and fragments of plagioclase in the middle part of the dykes (Laitakari 1969).

A review of the published data reveals that phenocryst assemblages have been reported for most of the known occurrences of Häme dykes (Laitakari 1969), whereas modal abundances have been reported for 17 dykes (Laitakari 1969, 1987), geochemical data have been published for 9 dykes (Savolahti 1956, 1966; Laitakari 1969; Boyd 1972; Lindqvist & Laitakari 1980; Laitakari 1987), and combined modal and geochemical data are available for three dykes (Ansio, Partakorpi, Lautaniemi). Examination of these data demonstrates that the WNW-trending set of dykes has 8–32 vol.% and the NW trending set has 2–38 vol.% of modal olivine. Moreover, 65 % of the WNW-trending dykes contain plagioclase phenocrysts or megacrysts, or both. The highest MgO contents in the WNW- and NW-trending sets are 12 wt.% and 8 wt.%, respectively. We conclude that these data are inconsistent with the widely adopted idea of a significant compositional difference between the two sets of dykes. It is important to point out that a subset of the WNW-trending dykes is compositionally distinctive. This group of dykes (Virmaila, Partakorpi, Torittu, Kellosalmi, Nikkaroinen) exhibits a diagnostic "spotted" texture (Laitakari 1969), has 19–32 vol.% of modal olivine, lacks plagioclase phenocrysts, exhibits the highest MgO contents, and includes the intrusion that was considered to manifest emplacement at ca. 1650 Ma (Vaasjoki & Sakko 1989). The spotted variety includes narrow dykes as well as some of the widest and most remarkable dykes of the swarm, which together constitute a single linear structure (Fig. 1).

We argue on the basis of these observations that, generalizing, the WNW- and NW-trending sets of dykes are not compositionally significantly different, and that the conventional scenario has been biased by data reported for the exceptional spotted type, which may well represent a single intrusion. Recent dating of the Virmaila dyke at ca. 1642 Ma (Salminen et al. 2017) further demonstrated that the age of the spotted dyke is indistinguishable from those of other dykes within analytical error.

Our geochemical data mainly represent rapidly cooled narrow dykes and dyke margins and facilitate comparison between the parental magmas that were emplaced into different sets of crustal fractures. In our dataset, the NW-trending and WNW-trending dykes correspond to the two main sets of dykes identified by Laitakari (1969) (Fig. S2 in Electronic Appendix C). Geochemical comparison between the groups does not indicate systematic differences and, in fact, our data demonstrate that the dykes with different strikes are remarkably similar. All of the dykes that have over 10 vol.% of modal olivine are more than 30 m wide (Laitakari 1969) and all of the samples with MgO > 6 wt.% are over 20 m wide. These observations and our accumulation model indicate that the olivine- and MgO-rich dykes do not record the intrusion of primitive, high-temperature magmas but rather that the enrichment in olivine and MgO results from crystal settling in slowly cooling intrusions (Fig. 5). We conclude that the parental magmas that were emplaced into the different crustal fracture sets were notably uniform low-MgO basalts. Moreover, the variations in incompatible element ratios, such as Nb/Y, La/Nb, and Zr/Y, cannot be correlated with different strikes (Fig. 6), which means that magmas formed by variable melting conditions and degrees of

crustal contamination were randomly emplaced in the different sets of crustal cracks. Importantly, examples from other dyke swarms demonstrate the development of similar mutually cross-cutting sets of dykes with two main orientations separated by an average acute angle of ca. 30° (e.g. Kjøll et al. 2019).

5.3. Geochronology of the Häme dyke swarm and associated silicic intrusions

A comparison of our new results and the previous age data for the rapakivi-related igneous rocks of southern Finland is displayed in Figure 7. The new concordant to nearly concordant $^{207}Pb/^{206}Pb$ ages for Häme dykes with various trends range from 1640 ± 6 Ma to 1635 ± 6 Ma. All of our dated samples represent low-Zr/Y dykes and their $^{207}Pb/^{206}Pb$ ages are identical within error to the combined upper intercept age 1639 ± 3 Ma that we interpret as the emplacement age of low-Zr/Y dykes H12, H13, H14, and H25. The ages of these dykes and their preferred common emplacement age are in line with the nearly concordant 1642 ± 2 Ma $^{207}Pb/^{206}Pb$ age of the Virmaila dyke (WNW, trend 95°E; Salminen et al. 2017) and the concordant, but relatively imprecise 1647 ± 14 Ma $^{207}Pb/^{206}Pb$ (LA-MC-ICPMS) age of the Torittu dyke (WNW, trend 95°E; Salminen et al. 2017). Given that both Virmaila and Torittu represent the spotted type of Laitakari (1969) and may well be segments of the same dyke (Fig. 1), we conclude the more precise age of the Virmaila dyke to record emplacement of the spotted dykes at ca. 1642 Ma. This age and our new ages also overlap with the combined 1646 ± 6 Ma U-Pb (TIMS) upper intercept age of the Heinola dyke (NW, trend 135°E, Laitakari 1987) and the Ansio dyke (NW, trend 135°E, Laitakari 1987). Geochemical data indicate these two dykes to be compositionally different, which renders the combined age of the Heinola and Ansio dykes unreliable. Only five of the ten fractions for these two dykes are nearly concordant, and all of the nearly concordant fractions represent the Ansio dyke (Laitakari 1987). We have calculated a new age of 1642 ± 10 Ma for Ansio (sample A808) with the assumption that the tabulated uncertainties in Laitakari (1987) are at the 2σ level. We conclude that the presently available age data for the Häme dykes are indistinguishable within error. Our results thus contradict the conventional view (Laitakari 1987; Vaasjoki & Sakko 1989) and support the suggestion of Salminen et al. (2017) that the NW- and WNW-trending dykes are broadly coeval with the emplacement ages ranging from 1642 ± 2 Ma to 1639 ± 3 Ma. It should be noted, however, that the 1642 ± 2 Ma Virmaila dyke and the 1642 ± 10 Ma Ansio dyke show affinity to high-Zr/Y dykes, which implies a possible small age difference between the low-Zr/Y dykes and high-Zr/Y dykes in the Häme swarm.

Our favored emplacement ages for the Häme mafic dykes are older than the proposed 1635–1628 Ma crystallization age of the Wiborg batholith (Heinonen et al. 2017), in accordance with earlier interpretations of age data and field observations (e.g. Laitakari 1969; Siivola 1987; Rämö & Mänttäri 2015). The ages of silicic dykes around the Wiborg batholith (1635 ± 2 Ma to 1619 ± 3 Ma; Rämö et al. 2014) and in the Sipoo swarm (1636 Ma; discordant U-Pb age of two fractions with 2σ errors of 12 Ma and 14 Ma; Törnroos 1984) demonstrate that silicic magmatic activity continued after the main period of magmatism in the Wiborg batholith. The occurrence of 1635 Ma bimodal composite dykes proves the continuation of mafic magmatism after the main pulse at ca. 1642 Ma (Rämö & Mänttäri 2015). Overall, the formation of the mafic and silicic intrusions of the Häme swarm and those associated with the Wiborg batholith can be dated between 1642 Ma and 1619 Ma.

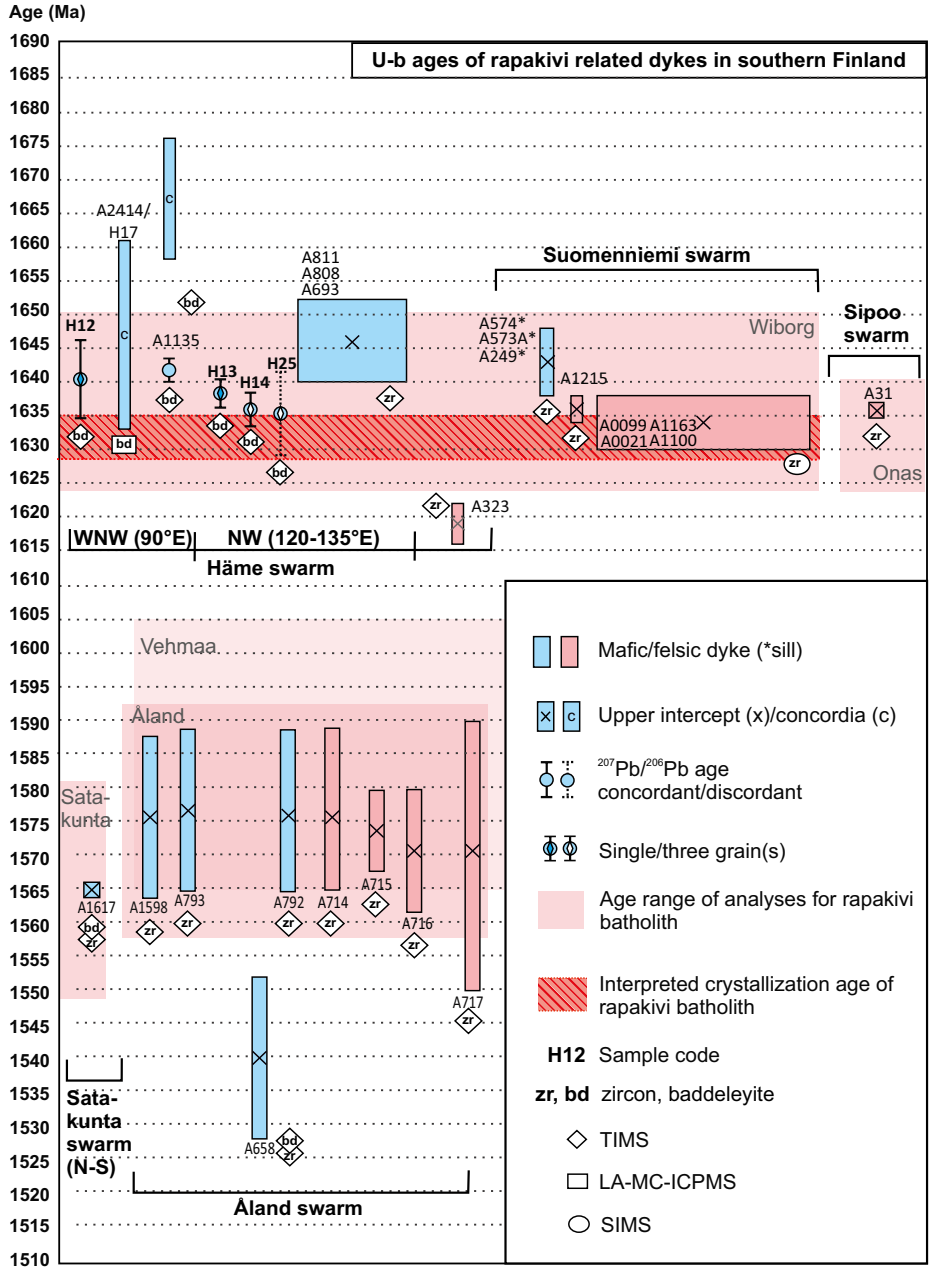

Figure 7. U-Pb age data for the mid-Proterozoic rapakivi-related magmatism in Finland. Age results for the mafic dykes (H12, H13, H14, and H 25) of the Häme swarm from this work are compared with previous results from (a) the Häme, Suomenniemi, and Sipoo swarms, and (b) the Satakunta and Åland swarms. The U–Pb age range for rapakivi batholiths (Vaasjoki 1977; Idman 1989; Suominen 1991; Lindberg & Bergman 1993; Lehtonen et al. 2003; Rämö et al. 2014; Heinonen et al. 2016; Heinonen et al. 2017) and interpreted crystallization age for Wiborg batholith are from Heinonen et al. (2017). The ages of mafic and silicic dykes are from A2414/H17 (Salminen et al. 2017), A1135 (Vaasjoki & Sakko 1989; Salminen et al. 2017); A693 (Laitakari 1987), A808 (Laitakari 1987), A811 (Laitakari 1987), A249 (Siivola 1987), A573A (Siivola 1987), A574 (Siivola 1987), A0021 (Rämö & Mänttäri 2015), A0099 (Rämö & Mänttäri 2015), A1100 (Rämö & Mänttäri 2015), A1163 (Rämö & Mänttäri 2015), A31 (Törnroos 1984), A1617 (Lehtonen et al. 2003), A1598 (Salminen et al. 2016), A793 (Suominen 1991), A658 (Suominen 1991), A792 (Suominen 1991), A71 (Suominen 1991), A715 (Suominen 1991), A716 (Suominen 1991), and A717 (Suominen 1991).

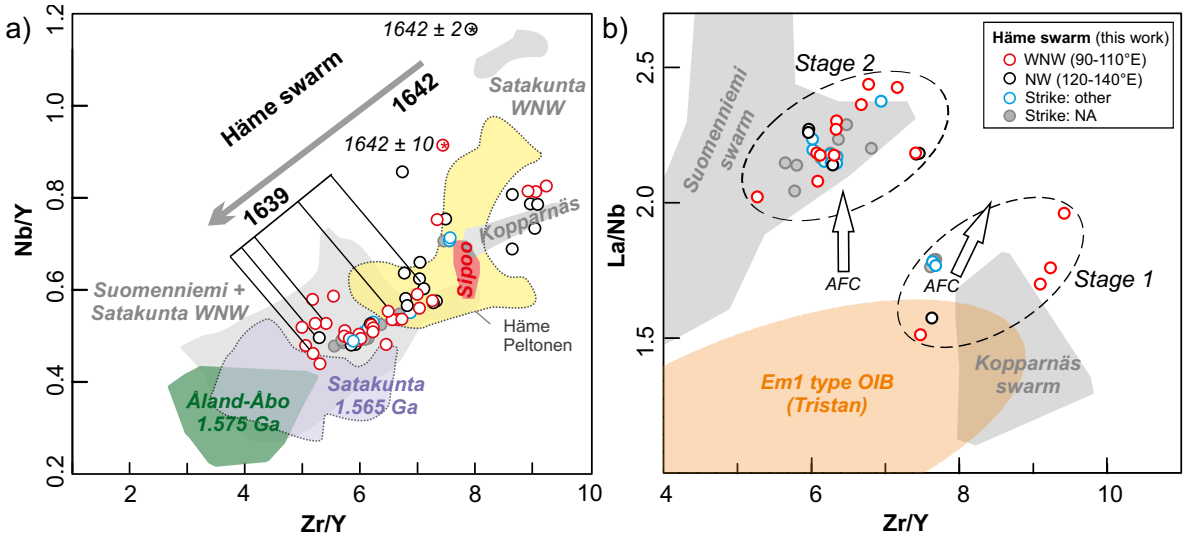

Figure 8. a) Variations in the Zr/Y and Nb/Y values and ages of the mid-Proterozoic mafic dyke swarms of southern Finland. The interpreted emplacement ages of the low-Zr/Y (1639 Ma, n = 5) and high-Zr/Y (1642 Ma, n = 2) –type dykes of the Häme dykes are indicated. (b) Geochemical distinction between postulated stage 1 and stage 2 of Häme dykes in a Zr/Y vs. La/Nb diagram. Compositional fields of the Kopparnäs dyke swarm and the Suomenniemi dyke swarm and modern EM1-affinity oceanic basalts from the Tristan da Cunha hotspot are presented for comparison. Arrows illustrate the compositional effect of crustal contamination due to combined assimilation and fractional crystallization (AFC). The La contents are based on ICP-MS and neutron activation methods. Data sources: this study, Rämö (1991), Luttinen & Kosunen (2006), Hoernle et al. (2015), Bohm (2018), Petri Peltonen (personal communication).

5.4. Origin of mid-Proterozoic mafic dyke swarms

5.4.1. Tentative three-stage model for mafic dyke swarms in southern Finland

The most reliable age data for the Häme dykes suggest emplacement of magmas during a relatively short period, and our geochemical data indicate that the parental magmas were quite uniform low-Mg tholeiites. Although the preferred ages are indistinguishable within analytical error, the dated high-Zr/Y-type, less contaminated dykes exhibit marginally older ages of ca. 1642 ± 2 Ma (Salminen et al. 2017) and 1642 ± 10 Ma (recalculated from Laitakari 1987) than the low-Zr/Y-type dykes dated at 1639 ± 3 Ma (Fig. 8). To provide a new working hypothesis for the origin of the mid-Proterozoic mafic dyke swarms in southern Finland, we presume the small age difference to be real.

Geochemically, the marginally older high-Zr/Y-type dykes tend to exhibit a weaker crustal contamination overprint (lower Th/Nb, La/Nb, Pb/Ce) than the much more abundant and younger low-Zr/Y-type dykes (Fig. 6), which is consistent with increasing degrees of melting of progressively heated wall-rocks. In the following discussion, we associate the high Zr/Y (and Nb/Y) and low Zr/Y (and Nb/Y) values with relatively lower and higher degrees of mantle melting, respectively, and link the degree of melting to the thickness of the continental lithosphere (section 5.1.). Our examination of the compositional variability in the mafic dyke swarms of southern Finland focuses on the Zr/Y values, because the Nb/Y values are more strongly influenced by mantle source compositions (solid–liquid distribution coefficients Y > Zr > Nb;

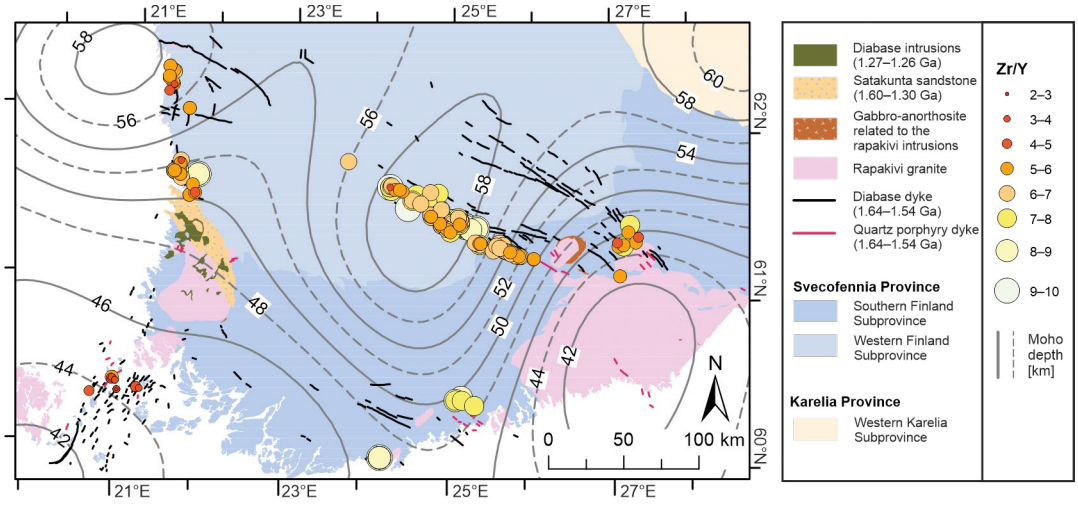

Figure 9. Spatial variability in the Zr/Y values of the rapakivi-related mafic dyke swarms of southern Finland. The MOHO depth is indicated (in km; Grad et al. 2009).

https://kdd.earthref.org/KdD/) and the Nb data tend to have larger errors in the compiled dataset, which mainly represents XRF analyses.

Comparison between the different mafic dyke swarms of southern Finland reveals that the Häme and Satakunta NW- to WNW-trending swarms (called Satakunta E-W in Salminen et al. 2014) exhibit a broadly similar wide range in Zr/Y. In contrast, the Sipoo and Kopparnäs swarms invariably have high Zr/Y, the Suomenniemi and Satakunta N–S-trending swarms are typified by moderately low Zr/Y, whereas the Åland–Åboland swarm has consistently low Zr/Y (Fig. 8). We explain the geochemical variability and ages of these mafic dyke swarms by a tentative three-stage model including: (1) an initial rifting stage, (2) a second stage of mantle melting under progressively thinning continental lithosphere, and (3) a late stage of intensive melting under thin lithosphere.

According to our model, the high-Zr/Y-type dykes represent the earliest stage of magmatism in the Häme dyke swarm and the first phase of mid-Proterozoic rapakivi-related magmatism in southern Finland at ca. 1642 Ma. The high-Zr/Y-type dykes of the Häme swarm occur in regions of thick crust (present-day MOHO depth >56 km; Fig. 9), and we associate their origin with relatively low degrees of mantle melting during the initial phase of rapakivi-related magmatism. Dykes with broadly similar high Zr/Y values are also found within a region of >50-km-thick crust in the Satakunta swarm (WNW trending) (Fig. 9) and, judging from the geochemical similarity (Fig. 8) and previous paleomagnetic studies (Salminen et al. 2014; Salminen et al. 2017), these undated dykes represent possible correlatives of the Häme dykes. In comparison, the high-Zr/Y dykes of the Sipoo, Kopparnäs, and Suomenniemi dyke swarms occur in regions of thinner crust (MOHO depth 45–50 km). Nonetheless, we assume that all of the high-Zr/Y (≥ 7.5)-type rapakivi-related mafic dykes in southern Finland represent the first stage of magmatism and mantle melting under thick lithosphere. We regard that the regions of thinned lithosphere and crust formed after the emplacement of the high-Zr/Y dykes.

Most of the Häme dykes, and the majority of the Suomenniemi dykes, have relatively low Zr/Y (and Nb/Y) values, and we associate their compositions with increased degrees of partial melting in upwelling mantle during lithospheric thinning and the second stage of anorogenic

magmatism at ca. 1639 Ma. Although the preferred 1643 ± 5 Ma age of the Suomenniemi dyke swarm (upper intercept U-Pb age of the Lovasjärvi sill intrusion; Siivola 1987) coincides with our first stage (Figs. 7 and 8), the average $^{207}Pb/^{206}Pb$ age of the least discordant fractions is 1638 ± 6 Ma, which would be in agreement with an affinity to the second stage. Furthermore, the low Sm/Yb values in the Lovasjärvi sill are suggestive of low Zr/Y values (ca. 6–7) typical of dykes correlated with the second stage (Zr data for the Lovasjärvi dyke are anomalous; Rämö 1991). The occurrences of the low-Zr/Y-type Häme dykes in the regions of thick lithosphere (Fig. 9) point to the lateral transport of magmas from the areas of thinned lithosphere where most of the magmas were probably generated. It is possible that at least some of the low-Zr/Y-type WNW- to NW-trending dykes of the Satakunta swarm correlate with these magmas (Figs. 8–9). Laitakari & Leino (1989) have previously suggested lateral flow of mafic magmas in the Häme swarm away from the Ahvenisto and Lovasjärvi intrusions on the basis of the occurrence of gabbroic and anorthositic autoliths and fragments in the dykes.

The transition from the first to the second stage probably represents increased magma production rates and heating of the crust. The degree of crustal contamination in the dykes can be estimated using contamination-sensitive incompatible element ratios, such as La/Nb. Examination of the La/Nb values is limited, however, by the scarcity of high-precision La analyses (ICP-MS and neutron activation), which are only available for the Häme, Suomenniemi, and Kopparnäs dyke swarms (Fig. 8). In the Häme swarm, the low-Zr/Y-type dykes typically have higher La/Nb values than the high-Zr/Y-type dykes, which we link to stronger crustal contamination of the low-Zr/Y magmas of the second stage (Fig. 8). The high-Zr/Y-type Kopparnäs dykes have low La/Nb values diagnostic of nearly uncontaminated compositions, whereas the Suomenniemi dykes show affinity to the crustally contaminated low-Zr/Y and high La/Nb Häme dykes, although the ratios extend to lower values. Rämö (1991) and (Luttinen & Kosunen 2006) have previously presented similar views on the Suomenniemi and Kopparnäs dyke swarms.

Our tentative model associates the increased amount of crustal contamination with gradual heating of the crust, which promoted melting of crustal wall rocks of mafic intrusions. The second stage culminated in the formation of silicic dykes and plutons within and adjacent to the Wiborg rapakivi batholith (Fig. 7; e.g. Heinonen et al. 2017). Field evidence for mingling and mixing proves the production of coeval mafic and silicic magmas (Rämö 1991; Salonsaari & Haapala 1994). Importantly, geochemical data for the mafic component of 1634 ± 4 Ma bimodal composite dykes associated with the Suomenniemi rapakivi pluton (Rämö & Mänttäri 2015) exhibit low-Zr/Y (7.3) and low-Nb/Y (0.51) compositions in accordance with our model (sample A1047; Rämö 1991).

The generation of the younger Åland–Åboland swarm represents the third stage of rapakivi-related mafic magmatism in southern Finland (Fig. 7). The highly discordant U–Pb data of the Åland–Åboland dyke swarm provide imprecise intercept ages from 1577 ± 12 Ma to 1540 ± 12 Ma (Suominen 1991) and cluster at ca. 1575 Ma. The Åland–Åboland dykes invariably have low Zr/Y and Nb/Y values and they occur within a region of thin lithosphere in southwestern Finland (Figs. 8–9). Some of the low-Zr/Y-type N–S-trending dykes of the nearby Satakunta swarm could have been transported from the Åland–Åboland region during this stage. In fact, one of the Satakunta dykes can be tentatively correlated with the Åland–Åboland dykes on the basis of the ca. 1565 Ma $^{207}Pb/^{206}Pb$ age of discordant baddeleyite analyses (Lehtonen et al. 2003), but trend and geochemical data for the dated unit are lacking. The U–Pb age data for the Vehmaa, Åland, and Laitila rapakivi plutons in southwestern Finland show overall contemporaneity with the Åland–Åboland dykes (Vaasjoki 1977; Idman 1989; Suominen 1991; Lindberg & Bergman 1993; Lehtonen et al. 2003), although the age data are quite imprecise (Fig. 7).

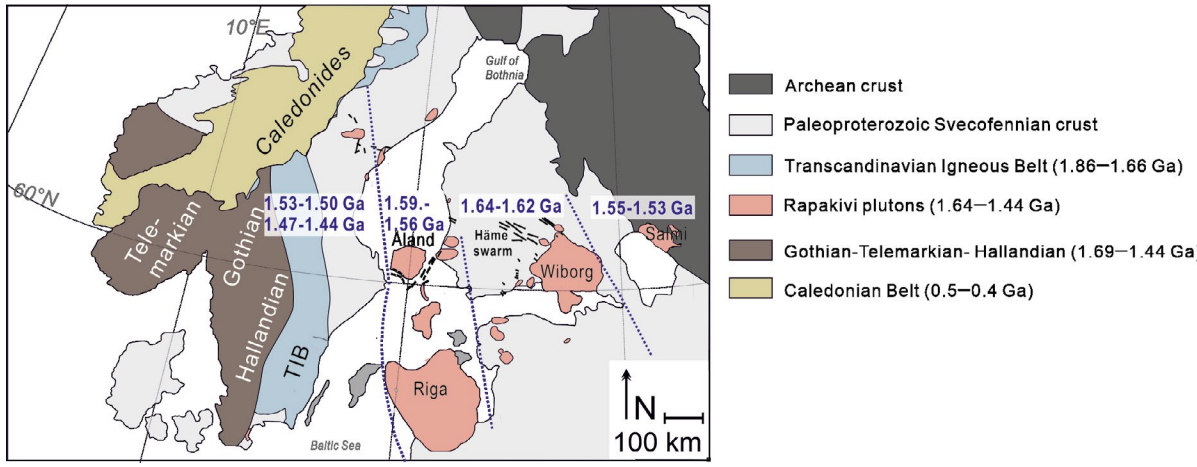

Figure 10. Major geological domains of the Fennoscandian Shield and spatial distribution of mid-Proterozoic 1670–1440 Ma magmatic rocks across Fennoscandia (modified from Korja et al. 2006; Ripa & Stephens 2020).

To conclude, the geochemical and geochronological data for the rapakivi-related mafic dykes of southern Finland are compatible with the generation of mantle-sourced mafic magmas by progressively higher degrees of partial melting in developing regions of thinned lithosphere. Generation of the silicic dyke swarms and voluminous rapakivi granite plutons can be attributed to extensive melting of heated crust during peaks of mafic intrusive activity during the envisioned second and third stages.

5.4.2. *Geodynamic setting of the mafic dyke swarms in southern Finland*

Evidence of an ultramature quartz arenitic sedimentary cover nonconformably overlying the Svecofennian metamorphic basement indicates that the onset of bimodal rapakivi-related magmatism at ca. 1640 Ma plausibly took place in an intracratonic rift-related environment (e.g. Pokki et al. 2013). The geodynamic setting and the causes of rifting and magmatism remain controversial, however, and both plate tectonic and mantle plume-related scenarios have been considered.

Several models have linked the rifting and magmatism to orogenic processes. One of the scenarios associates rapakivi-related magmatism with the long-term tectonic and thermal evolution of the thickened Svecofennian crust. After the termination of the regional compression that drove the Svecofennian orogeny, a gravitational collapse of the orogen took place at ca. 1800–1750 Ma (Korja et al. 2006). Widespread generation of post-collisional bimodal shoshonite-granite intrusions during the collapse may have been facilitated by radiogenic heat production within the thickened lithosphere (Kukkonen & Lauri 2009), or delamination of the lithospheric mantle (e.g. Väisänen et al. 2000), or both. It is theoretically possible that the subsequent bimodal rapakivi-related magmatism was similarly caused by the prolonged extensional collapse of the Svecofennian orogen (Windley 1993).

On the other hand, the formation of the rapakivi-related mafic and silicic magmas was coeval with the accretionary tectonics of the Gothian orogeny ca. 500–1000 km to the west (e.g. Åhäll et al. 2000; Ripa & Stephens 2020) (Fig. 10). Åhäll et al. (2000) emphasized that the 1690–1660 Ma, 1620–1580 Ma, and 1560–1550 Ma stages of the Gothian orogeny were each followed by a pulse of rapakivi-related magmatic activity in the Baltic Sea area. Furthermore, they suggested that the rapakivi-related magmatism and its temporal E–W zonation

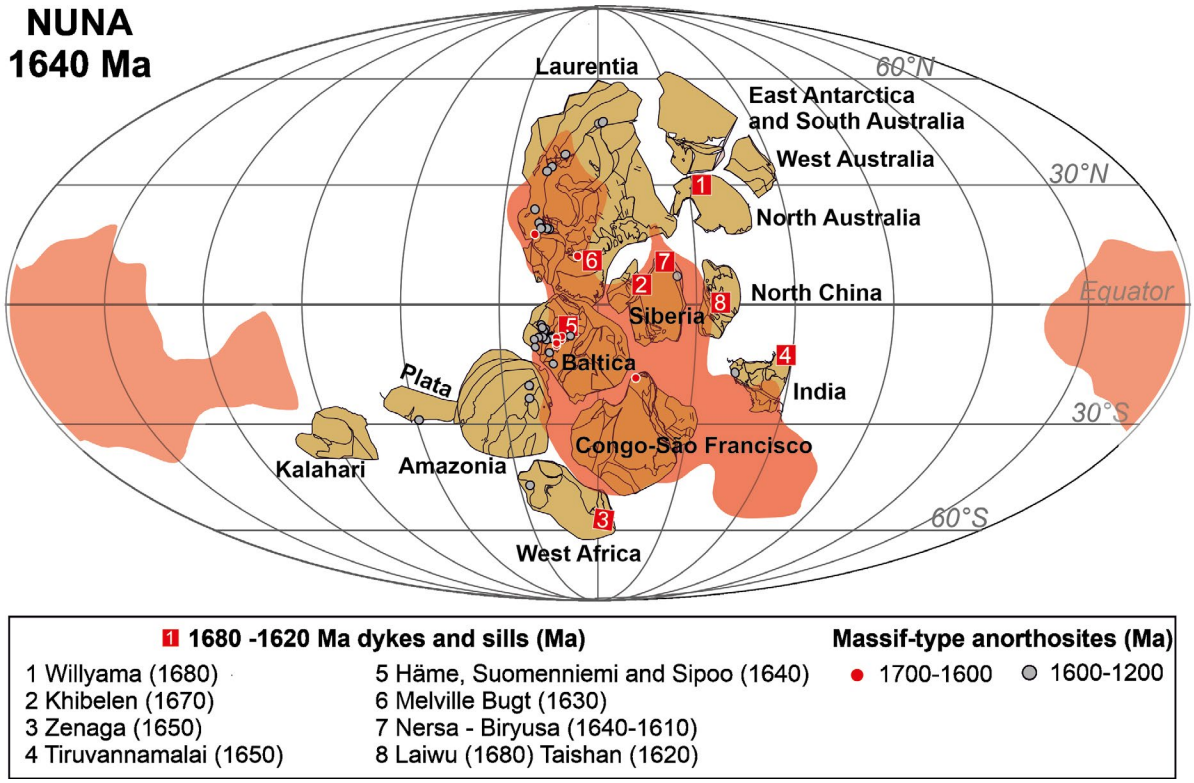

Figure 11. Reconstruction of the Nuna supercontinent at 1640 Ma (modified from Mitchell et al. 2021). The location of 1680–1620 Ma mafic dykes and sills (age in Ma in parentheses) (Ernst et al. 2013; Baratoux et al. 2019; Zhang et al. 2021) and 1700–1200 Ma massif-type anorthosites (Ashwal 1993, 2010) are indicated. The shapes of the present day African and Pacific large low-shear-velocity provinces (LLSVPs) at the core–mantle boundary are indicated with light red filling (1 % slow-velocity contour in the lowermost layer of the mean shear-wave tomographic model SMEAN, Becker & Boschi 2002). Nuna centered arbitrarily on zero meridian.

(Fig. 10) occurred in an extensional back-arc setting in response to recurring subduction in a westward-retreating mode. The formation of the 1547–1535 Ma Salmi batholith in the Lake Ladoga area does not comply with a simple spatial relationship between subduction roll-back and back-arc extension, however.

Mantle plume models for rapakivi-related rifting and magmatism have also been presented. For example, Pesonen et al. (1989) proposed that the bimodal magmatism resulted from the passage of the Fennoscandian Shield over a near-equatorial mantle plume. Furthermore, Halls et al. (2011) correlated the 2000-km-long Melville Bugt dyke swarm in SW Greenland and the Fennoscandian dyke swarms with a giant radiating dyke swarm system of a hypothetical plume-generated large igneous province. The most recent plate tectonic reconstructions do not support such a correlation, however (Fig. 11).

Available geochemical data on the Häme dykes and other rapakivi-related mafic rocks do not facilitate distinction between the plate tectonic and mantle plume scenarios. In the case of the Häme dyke swarm, the EM1-type mild enrichment of incompatible elements and the crustal fingerprints of the tholeiitic mafic rocks (Fig. 4 and Fig. S4 in Electronic Appendix C) could result from crustal contamination of magmas generated from the convective mantle in either a plate tectonic or a plume-related extensional setting. The relatively small scale and very long duration of rifting

and magmatism and the lack of age-progressive magmatic tracks in the rapakivi-related province of Fennoscandia do not conform with the presumed very large scale (ca. 2000 km diameter) and brief duration of plume-sourced magmatism (e.g. Bryan & Ernst 2008). Therefore, we favor the basic idea that the rapakivi-related magmatism was connected to plate tectonic processes, although deep mantle convection may have had a controlling influence on magma production (see section 5.4.3. below). Lithospheric extension related to the coeval Gothian orogeny seems to provide the most plausible explanation for the periodicity and age zonation of rapakivi-related magmatism (Åhäll et al. 2000).

5.4.3. The global context: Mid-Proterozoic mafic within-plate magmatism of the Nuna supercontinent

The worldwide occurrence of broadly coeval mid-Proterozoic within-plate magma systems is still not fully understood (e.g. Vigneresse 2005; Ashwal & Bybee 2017; Klausen & Nilsson 2019). The age range and geographic distribution of the ca. 1700–1200 Ma mafic dyke swarms and anorthosite suites manifest widespread mantle melting underneath the Nuna supercontinent soon after its amalgamation (Elming et al. 2021) (Fig. 11). Opinions differ as to whether the mafic magmas were derived from lithospheric or convective mantle and whether melting was driven by plate tectonics (e.g. Corrigan & Hanmer 1997; Scoates & Chamberlain 1997; Ashwal 2010) or deep mantle plumes (e.g. Emslie 1978; Hoffman 1989; Sharkov 2010). Regardless of the exact cause of melting, it may be important that the convective upper mantle underneath the regions of magmatic activity was probably heated by the insulation effect of the supercontinent (e.g. Hoffman 1989; Coltice et al. 2009). Anomalous hot upper mantle would help to explain the extensive degree of melting required for the production of voluminous tholeiites rather than minor alkaline melts underneath a thick continental lithosphere (e.g. Fitton & Upton 1987).

It may also be significant that these mid-Proterozoic igneous provinces were formed at relatively low latitudes, as Nuna apparently remained near the equator during this long period (e.g. Salminen et al. 2021). The deep mantle of the present-day Earth is typified by two colossal thermochemical anomalies, the so-called large low-shear-velocity provinces (LLSVPs; Garnero & McNamara 2008). They are equatorial to low-latitude (mainly within 30° N – 50° S) features that appear to have played a key role in both large-scale (large igneous provinces) and small-scale (e.g. kimberlite) plume-related magmatism through much of the Phanerozoic (Torsvik et al. 2010). LLSVPs may already have existed in the mid-Proterozoic (e.g. Doubrovine et al. 2016; Torsvik et al. 2016; Mitchell et al. 2021), and the upper mantle underneath Nuna could have been influenced by such a large-scale deep mantle anomaly. Consequently, the origin of the mid-Proterozoic dyke swarms and other within-plate igneous provinces may have been promoted by ascending hot convection currents from a deep LLSVP as well as supercontinent insulation above the mantle source region of the mafic magmas.

It is interesting to note that the mafic rocks of the mid-Proterozoic provinces frequently exhibit isotopic and chemical affinity to EM1 sources (e.g. Rämö 1991; Heinonen et al. 2010b; Bybee et al. 2015; Li et al. 2015; Wang et al. 2016; Klausen & Nilsson 2019; Gladkochub et al. 2021). The Phanerozoic EM1-affinity mafic rocks are characteristically associated with mantle plumes rooted in the sub-African LLSVP, and the EM1 component presumably represents the accumulation of subducted crustal material in deep mantle (e.g. Homrighausen et al. 2020). Similarly to the Fennoscandian rapakivi-related magmatic suites, however, many of the worldwide occurrences of mid-Proterozoic mafic dyke swarms, rapakivi granites, anorthosites, and associated rocks comprise relatively small within-plate provinces rather than large igneous provinces typical of

plume magmatism. We suspect plate tectonic processes had a controlling influence on their origins (e.g. Corrigan & Hanmer 1997; McLelland et al. 2010) by facilitating decompressional melting of exceptionally hot convective upper mantle. Widespread upwelling of relatively small mantle blobs rather than large plumes could have transported recycled EM1-type material from deep mantle to the base of the continental lithosphere underneath the mid-Proterozoic Nuna.

6. Conclusions

The mafic Häme dyke swarm exhibits two principal strike directions of NW (120–140°) and WNW (90–110°). Geochemical analyses of rapidly cooled parts of the dykes indicate notably uniform high-Ti tholeiitic and low-MgO parental magma compositions for the NW- and WNW-trending sets. The major element variations can be ascribed to the accumulation and fractionation of plagioclase and olivine phenocrysts.

Geochemically, the Häme dykes can be grouped on the basis of Zr/Y (and Nb/Y): judging from their high La/Nb (and Th/Nb, Pb/Ce) values, the predominant low-Zr/Y-type dykes are more strongly contaminated with crustal material than the high-Zr/Y-type dykes. The least-contaminated high-Zr/Y-type dykes are suggestive of an EM1-type mantle source for the Häme dyke swarm.

The upper intercept of four new ID-TIMS baddeleyite ages (1640 ± 6 Ma, 1635 ± 6 Ma, 1638 ± 2 Ma, and 1635 ± 3 Ma) suggests emplacement of low-Zr/Y-type dykes at 1639 ± 3 Ma. The previously reported 1642 ± 2 Ma (Salminen et al. 2017) and 1642 ± 10 Ma (recalculated from Laitakari 1987) ages imply a marginally older age for the high-Zr/Y-type dykes. In contrast with previous views, the strikes of the dykes do not correlate with their ages.

On a regional scale, we associate the variable Zr/Y and Nb/Y in the Häme dykes and other mafic dykes of southern Finland with vertical and lateral transport of magmas generated underneath relatively thick and thin lithospheric domains. Existing geochronological and geochemical data are compatible with a general progressive decrease in the Zr/Y values of mafic magmas generated within developing areas of thinned lithosphere. Prolonged, episodic mantle melting was triggered by extension possibly related to the coeval Gothian orogeny ca. 500–1000 km to the west (Åhäll et al. 2000) and was promoted by the heating of the convective upper mantle below the Nuna supercontinent.

A broadly similar geodynamic environment could apply to many of the widespread mid-Proterozoic mafic dyke swarms, rapakivi granites, anorthosites, and associated rocks that represent relatively small magma systems across Nuna. The hypothetical mid-Proterozoic equivalents of modern large low-shear-velocity provinces and related mantle plume generation zones in deep mantle represent additional potentially significant factors for widespread and high-degree mantle melting.

Acknowledgements

The authors acknowledge the funding from the Academy of Finland (129910 to A and 288277 to JS). This project contributes to the IGCP-648 project. Constructive feedback from the editor and two anonymous reviewers helped to improve the paper. Pasi Heikkilä is thanked for instructing the laboratory work for XRF analyses of KB and Robert Klein is thanked for picking the baddeleyite grains for geochronology. Petri Peltonen kindly provided unpublished reference data.

Supplementary data

Electronic Appendices A–C for this article are available via Bulletin of the Geological Society of Finland web page.
Electronic Appendix A: Häme diabase dyke samples.
Electronic Appendix B: Analytical data.
Electronic Appendix C: Supplementary figures.

References

Åhäll, K.-I. & Connelly, J., 1998. Intermittent 1.53–1.13Ga magmatism in western Baltica; age constraints and correlations within a postulated supercontinent. Precambrian Research 92, 1–20. https://doi.org/10.1016/S0301-9268(98)00064-3

Åhäll, K.-I., Connelly, J. N. & Brewer, T. S., 2000. Episodic rapakivi magmatism due to distal orogenesis?: Correlation of 1.69–1.50 Ga orogenic and inboard, "anorogenic" events in the Baltic Shield. Geology 28, 823–826. https://doi.org/10.1130/0091-7613(2000)28%3C823:ERMDTD%3E2.0.CO;2

Arndt, N. T., Czamanske, G. K., Wooden, J. L. & Fedorenko, V. A., 1993. Mantle and crustal contributions to continental flood volcanism. Tectonophysics 223, 39–52. https://doi.org/10.1016/0040-1951(93)90156-E

Ashwal, L. D., 1993. Anorthosites. Springer-Verlag Berlin Heidelberg, 422 p.

Ashwal, L. D., 2010. The temporaility of anorthosites. The Canadian Mineralogist 48, 711–728. https://doi.org/10.3749/canmin.48.4.711

Ashwal, L. D. & Bybee, G. M., 2017. Crustal evolution and the temporality of anorthosites. Earth-Science Reviews 173, 307–330. https://doi.org/10.1016/j.earscirev.2017.09.002.

Baratoux, L., Söderlund, U., Ernst, R. E., de Roever, E., Jessell, M. W., Kamo, S., Naba, S., Perrouty, S., Metelka, V., Yatte, D., Grenholm, M., Diallo, D. P., Ndiaye, P. M., Dioh, E., Cournède, C., Benoit, M., Baratoux, D., Youbi, N., Rousse, S. & Bendaoud, A., 2019. New U–Pb Baddeleyite Ages of Mafic Dyke Swarms of the West African and Amazonian Cratons: Implication for Their Configuration in Supercontinents Through Time. In: Srivastava, R. K., Ernst, R. E. & Peng, P. (Eds.), Dyke Swarms of the World: A Modern Perspective. Springer Singapore, Singapore, 263–314. https://doi.org/10.1007/978-981-13-1666-1_7

Becker, T. W. & Boschi, L., 2002. A comparison of tomographic and geodynamic mantle models. Geochemistry, Geophysics, Geosystems 3, 1003. https://doi.org/10.1029/2001GC000168.

Bellieni, G., Brotzu, P., Comin-Chiaramonti, P., Ernesto, M., Melfi, A. J., IPacca, I. G. & Piccirillo, E. M., 1984. Flood basalt to rhyolite suites in the southern Paraná plateau (Brazil): paleomagnetism, petrogenesis and geodynamic implications. Journal of Petrology 25, 579–618. https://doi.org/10.1093/petrology/25.3.579

Bohm, K., 2018. Geochemical and paleomagnetic constraints on mid-Proterozoic mafic dyke emplacement events in southern Finland. Master's thesis, University of Helsinki, 86 p.

Boyd, W. W. J., 1972. Diabase variation and genesis. Bulletin of the Geological Society of Finland 44, 21–34.

Boynton, W. V., 1984. Chapter 3 – Cosmochemistry of the Rare Earth Elements: Meteorite Studies. In: Henderson, P. (Ed.), Developments in Geochemistry. Elsevier, 63–114. https://doi.org/10.1016/B978-0-444-42148-7.50008-3

Bryan, S. E. & Ernst, R. E., 2008. Revised definition of Large Igneous Provinces (LIPs). Earth-Science Reviews 86, 175–202. https://doi.org/10.1016/j.earscirev.2007.08.008.

Bybee, G. M., Ashwal, L. D., Gower, C. F. & Hamilton, M. A., 2015. Pegmatitic Pods in the Mealy Mountains Intrusive Suite, Canada: Clues to the Origin of the Olivine–Orthopyroxene Dichotomy in Proterozoic Anorthosites. Journal of Petrology 56, 845–868. https://doi.org/10.1093/petrology/egv019.

Coltice, N., Bertrand, H., Rey, P., Jourdan, F., Phillips, B. R. & Ricard, Y., 2009. Global warming of the mantle beneath continents back to the Archaean. Gondwana Research 15, 254–266. https://doi.org/10.1016/j.gr.2008.10.001.

Corrigan, D. & Hanmer, S., 1997. Anorthosites and related granitoids in the Grenville orogen: A product of convective thinning of the lithosphere? Geology 25, 61–64. https://doi.org/10.1130/0091-7613.

Cox, K. G., Macdonald, R. & Hornung, G., 1967. Geochemical and petrographic provinces in the Karroo basalts of southern Africa. American Mineralogist 52, 1451–1474.

Doubrovine, P. V., Steinberger, B. & Torsvik, T. H., 2016. A failure to reject: Testing the correlation between large igneous provinces and deep mantle structures with EDF statistics. Geochemistry, Geophysics, Geosystems 17, 1130–1163. https://doi.org/10.1002/2015gc006044.

Eklund, O., Fröjdö, S. & Lindberg, B., 1994. Magma mixing, the petrogenetic link between anorthositic suites and rapakivi granites, Åland,SW Finland. Mineralogy and Petrology 50, 3–19. https://doi.org/10.1007/BF01160135.

Ellam, R. M., Carlson, R. W. & Shirey, S. B., 1992. Evidence from Re–Os isotopes for plume–lithosphere mixing in Karoo flood basalt genesis. Nature 359, 718–721. https://doi.org/10.1038/359718a0.

Elming, S.-Å., Salminen, J. & Pesonen, L. J., 2021. Chapter 16 – Paleo-Mesoproterozoic Nuna supercycle. In: Pesonen, L. J., Salminen, J., Elming, S.-Å., Evans, D. A. D. &Veikkolainen, T. (Eds.), Ancient Supercontinents and the Paleogeography of Earth. Elsevier, 499–548. https://doi.org/10.1016/B978-0-12-818533-9.00001-1

Emslie, R. F., 1978. Anorthosite massifs, rapakivi granites, and late proterozoic rifting of north America. Precambrian Research 7, 61–98. https://doi.org/10.1016/0301-9268(78)90005-0.

Ernst, R. E., Bleeker, W., Söderlund, U. & Kerr, A. C., 2013. Large Igneous Provinces and supercontinents: Toward completing the plate tectonic revolution. Lithos 174, 1–14. https://doi.org/10.1016/j.lithos.2013.02.017.

Fitton, J. G. & Upton, B. G. J., 1987. Introduction. Geological Society, London, Special Publications 30, ix. https://doi.org/10.1144/GSL.SP.1987.030.01.01.

Fred, R., Heinonen, A. & Heikkilä, P., 2019. Tracing the styles of mafic-felsic magma interaction: A case study from the Ahvenisto igneous complex, Finland. Bulletin of the Geological Society of Finland 91, 5–33. https://doi.org/10.17741/bgsf/91.1.001.

Frost, C. D. & Ronald Frost, B., 1997. Reduced rapakivi-type granites: The tholeiite connection. Geology 25, 647–650. https://doi.org/.1130/0091-7613.

Garnero, E. J. & McNamara, A. K., 2008. Structure and Dynamics of Earth's Lower Mantle. Science 320, 626. https://doi.org/10.1126/science.1148028.

Gibson, S. A., Thompson, R. N., Dickin, A. P. & Leonardos, O. H., 1995. High-Ti and low-Ti mafic potassic magmas: Key to plume-lithosphere interactions and continental flood-basalt genesis. Earth and Planetary Science Letters 136, 149–165. https://doi.org/10.1016/0012-821X(95)00179-G.

Gladkochub, D. P., Donskaya, T. V., Pisarevsky, S. A., Salnikova, E. B., Mazukabzov, A. M., Kotov, A. B., Motova, Z. L., Stepanova, A. V. & Kovach, V. P., 2021. Evidence of the latest Paleoproterozoic (~1615 Ma) mafic magmatism the southern Siberia: Extensional environments in Nuna supercontinent. Precambrian Research 354, 106049. https://doi.org/10.1016/j.precamres.2020.106049.

Grad, M., Tiira, T. & Group, E. S. C. W., 2009. The Moho depth map of the European Plate. Geophysical Journal International 176, 279–292. https://doi.org/10.1111/j.1365-246X.2008.03919.x.

Halls, H. C., Hamilton, M. A. & Denyszyn, S. W., 2011. The Melville Bugt Dyke Swarm of Greenland: A Connection to the 1.5–1.6 Ga Fennoscandian Rapakivi Granite Province? In: Srivastava, R. K. (Ed.), Dyke Swarms:Keys for Geodynamic Interpretation: Keys for Geodynamic Interpretation. Springer Berlin Heidelberg, Berlin, Heidelberg, 509–535. https://doi.org/10.1007/978-3-642-12496-9_27.

Hawkesworth, C. J., Marsh, J. S., Duncan, A. R., Erlank, A. J. & Norry, M. J., 1984. The role of continental lithosphere in the generation of the Karoo volcanic rocks: evidence from combined Nd-and Sr-isotope studies. Special Publication Geological Society South Africa 13, 341–354.

Heinonen, A., Mänttäri, I., Rämö, O. T., Andersen, T. & Larjamo, K., 2016. A priori evidence for zircon antecryst entrainment in megacrystic Proterozoic granites. Geology 44, 227–230. https://doi.org/10.1130/G37696.1.

Heinonen, A. P., Andersen, T. & Rämö, O. T., 2010a. Re-evaluation of Rapakivi Petrogenesis: Source Constraints from the Hf Isotope Composition of Zircon in the Rapakivi Granites and Associated Mafic Rocks of Southern Finland. Journal of Petrology 51, 1687–1709. https://doi.org/10.1093/petrology/egq035.

Heinonen, A. P., Rämö, O. T., Mänttäri, I., Johanson, B. & Alviola, R., 2010b. Formation and fractionation of high-Al tholeiitic magmas in the Ahvenisto rapakivi granite-massif-type anorthosite complex, Southern Finland. The Canadian Mineralogist 48, 969–990. https://doi.org/10.3749/canmin.48.4.969.

Heinonen, A. P., Rämö, O. T., Mänttäri, I., Andersen, T. & Larjamo, K., 2017. Zircon as a Proxy for the Magmatic Evolution of Proterozoic Ferroan Granites; the Wiborg Rapakivi Granite Batholith, SE Finland. Journal of Petrology 58, 2493–2517. https://doi.org/10.1093/petrology/egy014.

Heinonen, J. S., Luttinen, A. V., Spera, F. J. & Bohrson, W. A., 2019. Deep open storage and shallow closed transport system for a continental flood basalt sequence revealed with Magma Chamber Simulator. Contributions to Mineralogy and Petrology 174, 87. https://doi.org/10.1007/s00410-019-1624-0.

Hoernle, K., Rohde, J., Hauff, F., Garbe-Schönberg, D., Homrighausen, S., Werner, R. & Morgan, J. P., 2015. How and when plume zonation appeared during the 132 Myr evolution of the Tristan Hotspot. Nature Communications 6, 7799. https://doi.org/10.1038/ncomms8799.

Hoffman, P. F., 1989. Speculations on Laurentia's first gigayear (2.0 to 1.0 Ga). Geology 17, 135–138. https://doi.org/10.1130/0091-7613.

Hollocher, K., Robinson, P., Walsh, E. & Roberts, D., 2012. Geochemistry of amphibolite-facies volcanics and gabbros of the Støren Nappe in extensions west and southwest of Trondheim, Western Gneiss Region, Norway: a key to correlations and paleotectonic settings. American Journal of Science 312, 357–416. https://doi.org/10.2475/04.2012.01.

Homrighausen, S., Hoernle, K., Zhou, H., Geldmacher, J., Wartho, J. A., Hauff, F., Werner, R., Jung, S. & Morgan, J. P., 2020. Paired EMI-HIMU hotspots in the South Atlantic—Starting plume heads trigger compositionally distinct secondary plumes? Science Advances 6, eaba0282. https://doi.org/10.1126/sciadv.aba0282.

Idman, H., 1989. The Siipyy granite – A new rapakivi occurrence in Finland. Bulletin of the Geological Society of Finland 61, 123–127.

Jaffey, A. H., Flynn, K. F., Glendenin, L. E., Bentley, W. C. & Essling, A. M., 1971. Precision Measurement of Half-Lives and Specific Activities of ^{235}U and ^{238}U. Physical Review C 4, 1889–1906. https://doi.org/10.1103/PhysRevC.4.1889.

Janoušek, V., Farrow, C. M. & Erban, V., 2006. Interpretation of Whole-rock Geochemical Data in Igneous Geochemistry: Introducing Geochemical Data Toolkit (GCDkit). Journal of Petrology 47, 1255–1259. https://doi.org/10.1093/petrology/egl013.

Karlstrom, K. E., Åhäll, K.-I., Harlan, S. S., Williams, M. L., McLelland, J. & Geissman, J. W., 2001. Long-lived (1.8–1.0 Ga) convergent orogen in southern Laurentia, its extensions to Australia and Baltica, and implications for refining Rodinia. Precambrian Research 111, 5–30.

https://doi.org/10.1016/S0301-9268(01)00154-1.

Kjøll, H. J., Galland, O., Labrousse, L. & Andersen, T. B., 2019. Emplacement mechanisms of a dyke swarm across the brittle-ductile transition and the geodynamic implications for magma-rich margins. Earth and Planetary Science Letters 518, 223–235. https://doi.org/10.1016/j.epsl.2019.04.016.

Klausen, M. B. & Nilsson, M. K. M., 2019. The Melville Bugt Dyke Swarm across SE Greenland: A closer link to Mesoproterozoic AMCG-complexes. Precambrian Research 329, 88–107. https://doi.org/10.1016/j.precamres.2018.06.001.

Knaack, C., Cornelius, S. B. & Hooper, P. R., 1994. Trace Element Analyses of Rocks and Minerals by ICP-MS. GeoAnalytical Lab, Washington State University. http://www.sees.wsu.edu/Geolab/equipment/icpms.html.

Korja, A., Lahtinen, R. & Nironen, M., 2006. The Svecofennian orogen: a collage of microcontinents and island arcs. Geological Society, London, Memoirs 32, 561–578. 10.1144/gsl.Mem.2006.032.01.34.

Korsman, K., Korja, T., Pajunen, M. & Virransalo, P., 1999. The GGT/SVEKA Transect: Structure and Evolution of the Continental Crust in the Paleoproterozoic Svecofennian Orogen in Finland. International Geology Review - INT GEOL REV 41, 287–333. https://doi.org/10.1080/00206819909465144.

Kosunen, P., 1999. The rapakivi granite plutons of Bodom and Obbnäs, southern Finland: petrography and geochemistry. Bulletin of The Geological Society of Finland 71, 275–304.

Kukkonen, I. & Lauri, L., 2009. Modelling the thermal evolution of a collisional Precambrian orogen: High heat production migmatitic granites of southern Finland. Precambrian Research 168, 233–246. https://doi.org/10.1016/j.precamres.2008.10.004.

Lahtinen, R., Korja, A. & Nironen, M., 2005. Palaeoproterozoic tectonic evolution of the Fennoscandian Shield. In: Lehtinen, M., Nurmi, P. A. &Rämö, O. T. (Eds.), Precambrian Geology of Finland – Key to the Evolution of the Fennoscandian Shield. Developments in Precambrian Geology, 418–532.

Laitakari, I., 1969. On the set of olivine diabase dikes in Häme, Finland. Bulletin de la Commission Géologique de la Finlande 241, 65.

Laitakari, I., 1987. Hämeen subjotuninen diabaasijuoniparvi. Abstract: The Subjotnian diabase dyke swarm of Häme. In: Aro, K. & Laitakari, I. (Eds.), Suomen diabaasit ja muut emäksiset juonikivilajit (Diabases and other mafic dyke rocks in Finland). Geological Survey of Finland, Report of Investigation 76, 99–166.

Laitakari, I. & Leino, H., 1989. A New model for the emplacement of the Häme diabase dyke swarm, Central Finland. In: Autio, S. (Ed.), Current Research 1988, Geological Survey of Finland, Special Paper 10, 7–8.

Laitakari, I., Rämö, O., Suominen, V., Niin, M., Stepanov, K. & Amantov, A., 1996. Subjotnian: Rapakivi granites and related rocks in the suroundings of the Gulf of Finland. In: Koistinen, T. (Ed.), Explanation to the Map of Precambrian basement of the Gulf of Finland and surrounding area 1 : 1 mill. Special Paper – Geological Survey of Finland 21, 59–97.

Laitala, M., 1984. Pellingin ja Porvoon kartta-alueiden kallioperä (Summary: Pre-Quaternary rocks of the Pellinki and Porvoo map-sheet areas). Geological Map of Finland 1:100 000. Geological Survey of Finland, Explanation to the maps of pre-quaternary rocks, sheets 3012 and 3021 (in Finnish with English Summary), 53 p.

Lehtonen, M. I., Kujala, H., Kärkkäinen, N., Lehtonen, A., Mäkitie, H., Mänttäri, I., Virransalo, P. & Vuokko, J., 2003. Etelä-Pohjanmaan liuskealueen kallioperä. Summary: Pre-Quaternary rocks of the South Ostrobothnian Schist Belt. Geological Survey of Finland, Report of Investigation 158, 1–125.

Li, Y., Peng, P., Wang, X. & Wang, H., 2015. Nature of 1800–1600 Ma mafic dyke swarms in the North China Craton: Implications for the rejuvenation of the sub-continental lithospheric mantle. Precambrian Research 257, 114–123. https://doi.org/10.1016/j.precamres.2014.12.002.

Lindberg, B. & Bergman, L., 1993. Vehmaan kartta-alueen kallioperä (Summary: Pre-Quaternary rocks of the Vehmaa map-sheet area). Geological Map of Finland 1:100 000. Geological Survey of Finland, Explanation to the maps of Pre-Quaternary rocks, sheet 1042 (in Finnish with English Summary).

Lindholm, T., 2010. Hämeen diabaasijuonien geokemia. Master's thesis, University of Helsinki, 50 p.

Lindqvist, K. & Laitakari, I., 1980. Glass and amygdules in Precambrian diabases from Orivesi, southern Finland. Bulletin of the Geological Society of Finland 52, 221–229.

Ludwig, K. R., 2003. User's Manual for Isoplot 3.00 : A Geochronological Toolkit for Microsoft Excel. Revised August 27, 2003. ed, Berkeley CA :.

Luttinen, A. V. & Kosunen, P., 2006. The Kopparnäs dyke swarm in Inkoo, southern Finland: new evidence for Jothian magmatism in the SE Fennoscandian shield. In: Hanski, E., Mertanen, S., Rämö, T. & Vuollo, J. (Eds.), Dyke Swarms – Time Markers of Crustal Evolution. Taylor & Francis, 85–97.

Luttinen, A. V., Heinonen, J. S., Kurhila, M., Jourdan, F., Mänttäri, I., Vuori, S. K. & Huhma, H., 2015. Depleted Mantle-sourced CFB Magmatism in the Jurassic Africa–Antarctica Rift: Petrology and $^{40}Ar/^{39}Ar$ and U/Pb Chronology of the Vestfjella Dyke Swarm, Dronning Maud Land, Antarctica. Journal of Petrology 56, 919–952. https://doi.org/10.1093/petrology/egv022.

Luttinen, A., Lehtonen, E., Bohm, K., Lindholm, T., Salminen, J., 2022. Major and trace element analyses of diabase

dykes from Häme area, Southern Finland, Version 1.0. Interdisciplinary Earth Data Alliance (IEDA). https://doi.org/10.26022/IEDA/112310. Accessed 2022-05-26.

McLelland, J. M., Selleck, B. W., Hamilton, M. A. & Bickford, M. E., 2010. Late- to Post-tectonic setting of some major Proterozoic anorthosite-mangerite-charnokite-grante (AMCG) suites. The Canadian Mineralogist 48, 729–750. https://doi.org/10.3749/canmin.48.4.729.

Mitchell, R. N., Zhang, N., Salminen, J., Liu, Y., Spencer, C. J., Steinberger, B., Murphy, J. B. & Li, Z.-X., 2021. The supercontinent cycle. Nature Reviews Earth & Environment 2, 358–374. https://doi.org/10.1038/s43017-021-00160-0.

Nikkilä, K., Mänttäri, I., Nironen, M., Eklund, O. & Korja, A., 2016. Three stages to form a large batholith after terrane accretion – An example from the Svecofennian orogen. Precambrian Research 281, 618–638. https://doi.org/10.1016/j.precamres.2016.06.018.

Nironen, M., 2017. Guide to geological map of Finland – Bedrock 1:1000000. In: Nironen, M. (Ed.), Bedrock of Finland at the scale 1:1 000 000 – Major stratigraphic units, metamorphism and tectonic evolution. 60, 41–76.

Pearce, J. A., 2008. Geochemical fingerprinting of oceanic basalts with applications to ophiolite classification and the search for Archean oceanic crust. Lithos 100, 14–48. https://doi.org/10.1016/j.lithos.2007.06.016.

Pesonen, L. J., Torsvik, T. H., Elming, S. Å. & Bylund, G., 1989. Crustal evolution of Fennoscandia—palaeomagnetic constraints. Tectonophysics 162, 27–49. https://doi.org/10.1016/0040-1951(89)90355-7.

Pik, R., Deniel, C., Coulon, C., Yirgu, G., Hoffmann, C. & Ayalew, D., 1998. The northwestern Ethiopian Plateau flood basalts: classification and spatial distribution of magma types. Journal of Volcanology and Geothermal Research 81, 91–111.

Pokki, J., Kohonen, J., Rämö, O. T. & Andersen, T., 2013. The Suursaari conglomerate (SE Fennoscandian shield; Russia)—Indication of cratonic conditions and rapid reworking of quartz arenitic cover at the outset of the emplacement of the rapakivi granites at ca. 1.65 Ga. Precambrian Research 233, 132–143. https://doi.org/10.1016/j.precamres.2013.04.008.

Rämö, O. T., 1991. Petrogenesis of the Proterozoic rapakivi granites and related basic rocks of southeastern Fennoscandia: Nd and Pb istopic and general geochemical constraints. Geological Survey of Finland, Bulletin 355, 1–161.

Rämö, O. T. & Haapala, I., 1995. One hundred years of rapakivi granite. Mineralogy and Petrology 52, 129–185. https://doi.org/10.1016/j.lithos.2007.06.01610.1007/BF01163243.

Rämö, O. T. & Haapala, I., 2005. Chapter 12 Rapakivi Granites. In: Lehtinen, M., Nurmi, P. A. & Rämö, O. T. (Eds.), Developments in Precambrian Geology. Elsevier, 533–562. https://doi.org/10.1016/S0166-2635(05)80013-1

Rämö, O. T., Turkki, V., Mänttäri, I., Heinonen, A. P., Larjamo, K. & Lahaye, Y., 2014. Age and isotopic fingerprints of some plutonic rocksin the Wiborg rapakivi granite batholith with specialreference to the dark wiborgite of the Ristisaari Island. Bulletin of the Geological Society of Finland 86, 71–91.

Rämö, O. T. & Mänttäri, I., 2015. Geochronology of the Suomenniemi rapakivi granite complex revisited: Implications of point-specific errors on zircon U-Pb and refined λ87 on whole-rock Rb-Sr. Bulletin of the Geological Society of Finland 87, 25-45. https://doi.org/10.1016/j.lithos.2007.06.01610.17741/bgsf/87.1.002.

Rämö, O. T., Heikkilä, P. A. & Pulkkinen, A. H., 2016. Geochemistry of Paraná-Etendeka basalts from Misiones, Argentina: Some new insights into the petrogenesis of high-Ti continental flood basalts. Journal of South American Earth Sciences 67, 25–39. https://doi.org/10.1016/j.lithos.2007.06.01610.1016/j.jsames.2016.01.008.

Riley, T. R., Leat, P. T., Curtis, M. L., Millar, I. L., Duncan, R. A. & Fazel, A., 2005. Early–Middle Jurassic Dolerite Dykes from Western Dronning Maud Land (Antarctica): Identifying Mantle Sources in the Karoo Large Igneous Province. Journal of Petrology 46, 1489–1524. https://doi.org/10.1093/petrology/egi023.

Ripa, M. & Stephens, M. B., 2020. Chapter 10 Magmatism (1.6–1.4 Ga) and Mesoproterozoic sedimentation related to intracratonic rifting coeval with distal accretionary orogenesis. Geological Society, London, Memoirs 50, 269–288. https://doi.org/10.1144/m50-2017-4.

Rudnick, R. L. & Gao, S., 2003. Composition of the continental crust. Treatise on Geochemistry 3, 1–64.

Salminen, J., Mertanen, S., Evans, D. A. D. & Wang, Z., 2014. Paleomagnetic and geochemical studies of the Mesoproterozoic Satakunta dyke swarms, Finland, with implications for a Northern Europe – North America (NENA) connection within Nuna supercontinent. Precambrian Research 244, 170–191. https://doi.org/10.1016/j.precamres.2013.08.006.

Salminen, J., Klein, R., Mertanen, S., Pesonen, L. J., Fröjdö, S., Mänttäri, I. & Eklund, O., 2016. Palaeomagnetism and U–Pb geochronology ofc.1570 Ma intrusives from Åland archipelago, SW Finland – implications for Nuna. Geological Society, London, Special Publications 424, 95–118. https://doi.org/10.1144/sp424.3.

Salminen, J., Klein, R., Veikkolainen, T., Mertanen, S. & Mänttäri, I., 2017. Mesoproterozoic geomagnetic reversal asymmetry in light of new paleomagnetic and geochronological data for the Häme dyke swarm, Finland: Implications for the Nuna supercontinent. Precambrian Research 288, 1–22. https://doi.org/10.1016/j.precamres.2016.11.003.

Salminen, J., Lehtonen, E., Mertanen, S., Pesonen, L. J., Elming, S.-Å. & Luoto, T., 2021. Chapter 5 – The

Precambrian drift history and paleogeography of Baltica. In: Pesonen, L. J., Salminen, J., Elming, S.-Å., Evans, D. A. D. &Veikkolainen, T. (Eds.), Ancient Supercontinents and the Paleogeography of Earth. Elsevier, 155–205. https://doi.org/10.1016/B978-0-12-818533-9.00015-1.

Salonsaari, P. T. & Haapala, I., 1994. The Jaala-Iitti rapakivi complex. An example of bimodal magmatism and hybridization in the Wiborg rapakivi batholith, southeastern Finland. Mineralogy and Petrology 50, 21–34. https://doi.org/10.1007/BF01160136.

Savolahti, A., 1956. The Ahvenisto Massif in Finland. Bulletin de la Commission Géologique de Finlande 174, 1–96.

Savolahti, A., 1966. The differentiation of gabbro-anorthosite intrusions and the formation of anorthosites. Bulletin de la Commission Géologique de Finlande 222, 173–197.

Scoates, J. S. & Chamberlain, K. R., 1997. Orogenic to Post-Orogenic Origin For the 1.76 Ga Horse Creek Anorthosite Complex, Wyoming, Usa. The Journal of Geology 105, 331–344. https://doi.org/10.1086/515928.

Sharkov, E. V., 2010. Middle-proterozoic anorthosite–rapakivi granite complexes: An example of within-plate magmatism in abnormally thick crust: Evidence from the East European Craton. Precambrian Research 183, 689–700. https://doi.org/10.1016/j.precamres.2010.08.008.

Siivola, J., 1987. The mafic intrusion of Lovasjärvi. In: Aro, K. &Laitakari, I. (Eds.), Suomen diabaasit ja muut emäksiset juonikivilajit (Diabases and other mafic dyke rocks in Finland). Geological Survey of Finland, Report of Investigation 76, 121–128.

Söderlund, U. & Johansson, L., 2002. A simple way to extract baddeleyite (ZrO2). Geochemistry, Geophysics, Geosystems 3, 1 of 7–7 of 7. https://doi.org/10.1029/2001GC000212.

Stacey, J. S. & Kramers, J. D., 1975. Approximation of terrestrial lead isotope evolution by a two-stage model. Earth and Planetary Science Letters 26, 207–221. https://doi.org/10.1016/0012-821X(75)90088-6.

Steiger, R. H. & Jäger, E., 1977. Subcommission on geochronology: Convention on the use of decay constants in geo- and cosmochronology. Earth and Planetary Science Letters 36, 359–362. https://doi.org/10.1016/0012-821X(77)90060-7.

Sun, S. & McDonough, W. F., 1989. Chemical and isotopic systematics of oceanic basalts: implications for mantle composition and processes. Geological Society, London, Special Publications 42, 313–345. https://doi.org/10.1144/gsl.Sp.1989.042.01.19.

Suominen, V., 1991. The chronostratigraphy of southwestern Finland with special reference to Postjotnian and Subjotnian diabases, 100 p.

Törnroos, R., 1984. Petrography, Mineral Chemistry and Petrochemistry of Granite Porphyry Dykes from Sibbo, Southern Finland. Geological Survey of Finland, Bulletin 326, 43.

Torsvik, T. H., Burke, K., Steinberger, B., Webb, S. J. & Ashwal, L. D., 2010. Diamonds sampled by plumes from the core–mantle boundary. Nature 466, 352–355. https://doi.org/10.1038/nature09216.

Torsvik, T. H., Steinberger, B., Ashwal, L. D., Doubrovine, P. & Tronnes, R., 2016. Earth Evolution and Dynamics – A tribute to Kevin Burke. Canadian Journal of Earth Sciences 53. https://doi.org/10.1139/cjes-2015-0228.

Vaasjoki, M., 1977. Rapakivi granites and other postorogenic rocks in Finland: their age and the lead isotopic composition of certain associated galena mineralizations. Geological Survey of Finland Bulletin, 66.

Vaasjoki, M. & Sakko, M., 1989. The radiometric age of the Virmaila diabase dyke: evidence for 20 Ma of continental rifting in Padasjoki, southern Finland. In: Autio, S. (Ed.), Current Research 1988, Geological Survey of Finland, Special Paper 10, 43–44.

Vaasjoki, M., Sakko, M. & Rämö, T., 1989. New zircon age determinations from the Wiborg rapakivi batholit southeastern Finland. In: Autio, S. (Ed.), Current Research 1988, Geological Survey of Finland, Special Paper 10, 41–42.

Vaasjoki, M., Rämö, T. O. & Sakko, M., 1991. New U-Pb ages from the Wiborg rapakivi area: constraints on the temporal evolution of the rapakivi granite-anorthosite-diabase dyke association of southeastern Finland. Precambrian Research 51, 227–243. https://doi.org/10.1016/0301-9268(91)90102-G.

Väisänen, M., Mänttäri, I., Kriegsman, L. & Hölttä, P., 2000. Tectonic setting of post-collisional magmatism in the Palaeoproterozoic Svecofennian Orogen, SW Finland. Lithos 54, 63–81. https://doi.org.10.1016/S0024-4937(00)00018-9.

Vigneresse, J. L., 2005. The specific case of the Mid-Proterozoic rapakivi granites and associated suite within the context of the Columbia supercontinent. Precambrian Research 137, 1–34. https://doi.org/10.1016/j.precamres.2005.01.001.

Wang, C., Peng, P., Wang, X. & Yang, S., 2016. Nature of three Proterozoic (1680 Ma, 1230 Ma and 775 Ma) mafic dyke swarms in North China: Implications for tectonic evolution and paleogeographic reconstruction. Precambrian Research 285, 109–126. https://doi.org/10.1016/j.precamres.2016.09.015.

Willbold, M. & Stracke, A., 2006. Trace element composition of mantle end-members: Implications for recycling of oceanic and upper and lower continental crust. Geochemistry, Geophysics, Geosystems 7. https://doi.org/10.1029/2005GC001005.

Windley, B. F., 1993. Proterozoic anorogenic magmatism and its orogenic connections: Fermor Lecture 1991. Journal of the Geological Society 150, 39–50. https://doi.org/10.1144/gsjgs.150.1.0039

Zhang, S.-H., Ernst, R. E., Pei, J.-L., Zhao, Y. & Hu, G.-H., 2021. Large Igneous Provinces (LIPs) and Anoxia Events in "The Boring Billion". Large Igneous Provinces, 449–486. https://doi.org/10.1002/9781119507444.ch20.